AD-A162 890 BASIC AND APPLIED MAGNETISM WITH A SQUID GRADIOMETER (U) ILLINOIS INST OF TECH CHICAGO H WEINSTOCK ET AL. DEC 85 N00014-82-K-2042 1/1

UNCLASSIFIED F/G 14/2 NL

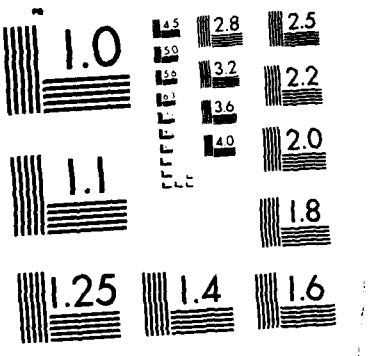

(1)

SECURITY CLASSIFICATION OF THIS PAGE

AD-A162 890

REPORT DOCUMENTATION PAGE

1a REPORT SECURITY CLASSIFICATION: Unclassified	1b RESTRICTIVE MARKINGS
2a SECURITY CLASSIFICATION AUTHORITY	3 DISTRIBUTION/AVAILABILITY OF REPORT: Public Release, Unlimited
DECLASSIFICATION/DOWNGRADING SCHEDULE	
PERFORMING ORGANIZATION REPORT NUMBER(S)	5. MONITORING ORGANIZATION REPORT NUMBER(S)
NAME OF PERFORMING ORGANIZATION: Illinois Institute of Technology; 6b OFFICE SYMBOL (If applicable)	7a. NAME OF MONITORING ORGANIZATION
ADDRESS (City, State and ZIP Code): Chicago, IL 60616	7b. ADDRESS (City, State and ZIP Code)
NAME OF FUNDING/SPONSORING ORGANIZATION: Naval Research Lab.; 8b OFFICE SYMBOL (If applicable): 6854	9. PROCUREMENT INSTRUMENT IDENTIFICATION NUMBER: Contract N00014-82-K-2042
ADDRESS (City, State and ZIP Code)	10 SOURCE OF FUNDING NOS.
TITLE (Include Security Classification)	PROGRAM ELEMENT NO. / PROJECT NO. / TASK NO / WORK UNIT NO

12 PERSONAL AUTHOR(S): Harold Weinstock ; M.N. Nisenoff; T. Erber

13a TYPE OF REPORT	13b. TIME COVERED	14 DATE OF REPORT (Yr., Mo., Day)	15 PAGE COUNT
Final	FROM 8/82 TO 8/83	1985 December	

16. SUPPLEMENTARY NOTATION

17 COSATI CODES			18. SUBJECT TERMS (Continue on reverse if necessary and identify by block number)
FIELD	GROUP	SUB. GR.	

19 ABSTRACT (Continue on reverse if necessary and identify by block number)

A facility was established at ~~the Naval~~ Research Lab. to evaluate the magnetic signatures of cryocoolers, i.e., small closed-cycle liquid helium refrigerators, by use of a (superconducting) SQUID gradiometer. This gradiometer also was utilized to study the (1) threshold of Barkhausen emission and onset of hysteresis in iron, (2) detection of defects in metal pipes by remote sensing, and (3) magnetoelastic behavior in steel bars.

20 DISTRIBUTION AVAILABILITY OF ABSTRACT	21 ABSTRACT SECURITY CLASSIFICATION
UNCLASSIFIED/UNLIMITED ☒ SAME AS RPT ☐ DTIC USERS ☐	Unclassified
22a NAME OF RESPONSIBLE INDIVIDUAL: M.N. Nisenoff	22b TELEPHONE NUMBER (Include Area Code): 202-767-3099 / 22c OFFICE SYMBOL: 6854

DD FORM 1473, 83 APR EDITION OF 1 JAN 73 IS OBSOLETE

SECURITY CLASSIFICATION OF THIS PAGE

DTIC FILE COPY

DTIC ELECTE JAN 6 1986 S D

B

85 12 31 026

FINAL REPORT

BASIC AND APPLIED MAGNETISM WITH A SQUID GRADIOMETER

Contract No. N00014-82-K-2042
August 1982 to August 1983

Prepared for

THE NAVAL RESEARCH LABORATORY (NRL)
Code 6854
4555 Overlook Ave., S.W.
Washington, DC 20375

Prepared by

Harold Weinstock
Illinois Institute of Technology
Chicago, IL 60616

INTRODUCTION

There is recent increasing interest in the use of superconductive electronics for Navy systems. Accordingly, there is a strong need for small closed-cycle liquid helium refrigerators (known as cryocoolers). However, there is concern about possible interference between sensitive magnetic instrumentation and the magnetic signature of cryocoolers.

The goal of this activity was to establish a facility at the Naval Research Laboratory (NRL) which would utilize a SQUID magnetic gradiometer to evaluate the magnetic signatures of candidate cryocoolers supplied to NRL under an Office of Naval Research (ONR) program for the design and construction of small cryocoolers. Specifically, the following tasks were to be performed:

(a) A facility was to be established at NRL in the best possible site to minimize noise, and the effective (SQUID) instrument noise level was to be determined.

(b) Measurements of the magnetic signatures of the candidate cryocoolers were to be made with the aim of identifying the exact origin of the signals received and subsequently recommending how such signals might be suppressed by a more judicious choice of construction materials and/or magnetic shielding.

In addition to the above activity, the instrumentation (when installed) was to be utilized to explore various new magnetic techniques of non-destructive testing of materials.

RESULTS

1. Magnetic Test Facility

After considerable exploration throughout NRL, it was determined that several locations provided minimal environmental magnetic noise.

For convenience, one of those locations, room 201, in building 208, was chosen for the installation. This installation was found to be suitable for the intended purpose of measuring cryocooler signatures. Background noise for the SQUID gradiometer was on the order of 10^{-9} gauss/$Hz^{\frac{1}{2}}$ for a band pass of 0 - 10 Hz, which is about that stated by the manufacturer as due to instrumental noise. No cryocoolers were delivered to NRL during the period of performance, and thus none could be evaluated.

2. Barkhausen Noise

The major research activity involved a study of Barkhausen emission and hysteresis in polycrystalline and single crystal samples of pure iron. These studies reveal the history-dependent nature of magnetic cycling and have led to a new understanding of irreversible magnetic behavior. This, in turn, may have an impact on the ability to (1) extract information from magnetic tapes and (2) demagnetize submarines and other vehicles comprised of ferromagnetic structural elements. A complete description of this research is provided in the two publications which are appended to this report. The more comlete publication entitled "Threshold of Barkhausen Emission and Onset of Hysteresis in Iron" has been accepted by the Physical Review; the shorter publication entitled "SQUID Detection of Barkhausen Threshold and Magnetic Kaiser Effect" has been accepted for presentation at the XVII International Conference on Low Temperature Physics (15-22 August 1984 at Karlsruhe, West Germany) and has now been published.

3. Defect Detection in Pipes

The SQUID gradiometer was utilized also to detect structural defects and anomalies in pipes, while the gradiometer itself was separated from the pipes being tested by distances ranging from several inches to over two feet. This was done by passing low frequency ($\sim$ 5 Hz) current through the pipes and observing changes in the amplitude of the associated magnetic field as

a pipe is passed beneath the gradiometer. The technique described could be applied to searches for holes and cracks in buried pipelines, the piping in ships' power plants and nuclear reactors. See Figures 1 and 2 for a schematic drawing of this application and some results obtained.

4. Magnetoelastic Effect

A final application of SQUID gradiometry involved the observation of changes in magnetic field in the vicinity of ferromagnetic (steel) bars being strained both below and above the elastic limit. Since there is a change in sign of the magnetoelastic coefficient for iron-based alloys at a strain level not far below the elastic limit, there is a dramatic reversal in the slope of the strain vs. flux-change curve at the point where the coefficient changes sign. Furthermore, upon exceeding the elastic limit, this same slope changes qualitatively. Thus, by providing some means of cyclic strain, observation of the phase relation between strain and flux change should enable one to tell immediately whether the structural element being tested is on one side or the other of the strain for which the magnetoelastic coefficient reverses. If on the low strain side, it would be known that the elastic limit has not been exceeded. If on the high strain side, it would be known that the elastic limit has been either closely approached or exceeded. Calibration of the SQUID signal as a function of distance might even enable one to determine whether the slope observed is characteristic of elastic or plastic behavior. There is some evidence that magnetic gradiometry could even be used to determine changes of residual strain in structural elements. See Figure 3 for one set of results obtained in which stress and change in magnetic flux are recorded as a function of strain for a cold-rolled steel bar. The bottom of the SQUID dewar was over 8" from the bar at a 45° angle, and the SQUID circuitry was on the x 1 (i.e., least sensitive) scale.

FIGURE CAPTIONS

Figure 1: (a) Cross-sectional view of dewar and sample iron pipe with two test holes. Pipe was moved horizontally (along its own axis).

(b) Top view of pipe showing configuration of the two holes.

Figure 2: Peak-to-peak response of SQUID circuit output when about 1 A (rms) at 4.8 Hz was passed through the pipe with the configuration as shown in Figure 1.

Figure 3: Stress and change in magnetic flux as a function of strain for a cold-rolled steel bar. The numbers shown refer to successive cycles.

(a)

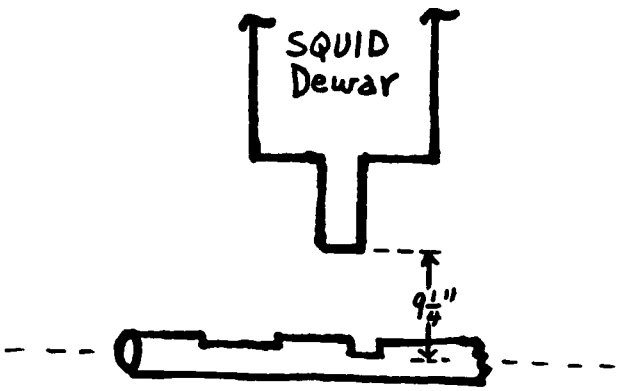

(b)

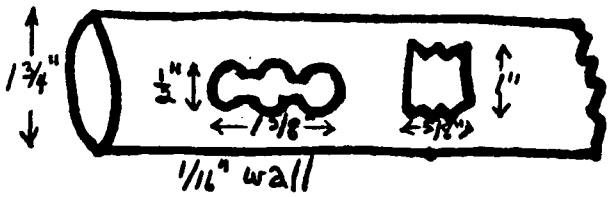

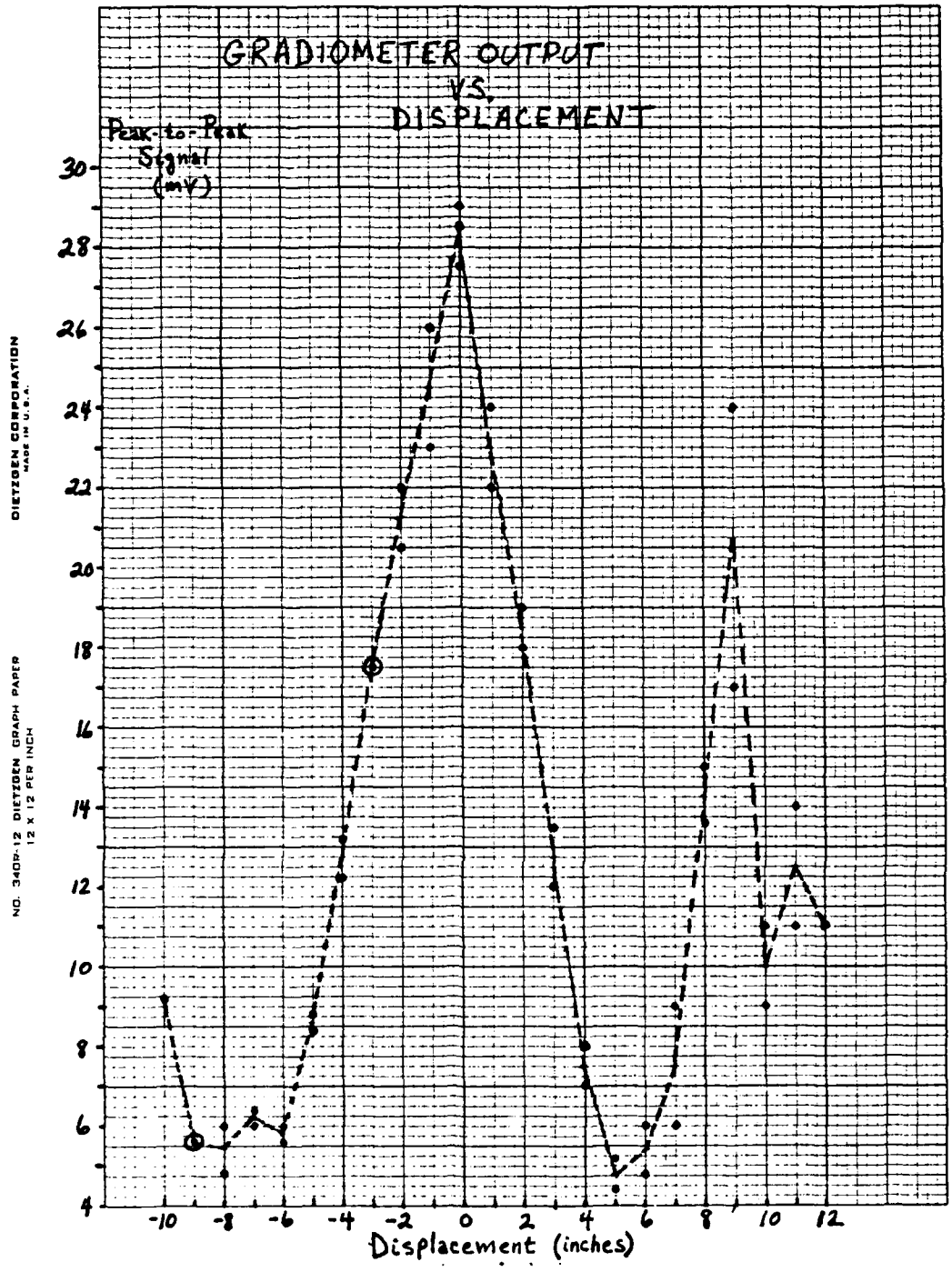
GRADIOMETER OUTPUT
VS.
DISPLACEMENT
Peak-to-Peak
Signal
(mV)
30
28
26
24
22
20
18
16
14
12
10
8
6
4
-10
-8
-6
-4
-2
0
2
4
6
8
10
12
Displacement (inches)
DIETZGEN CORPORATION
MADE IN U.S.A.
NO. 340R-12 DIETZGEN GRAPH PAPER
12 X 12 PER INCH

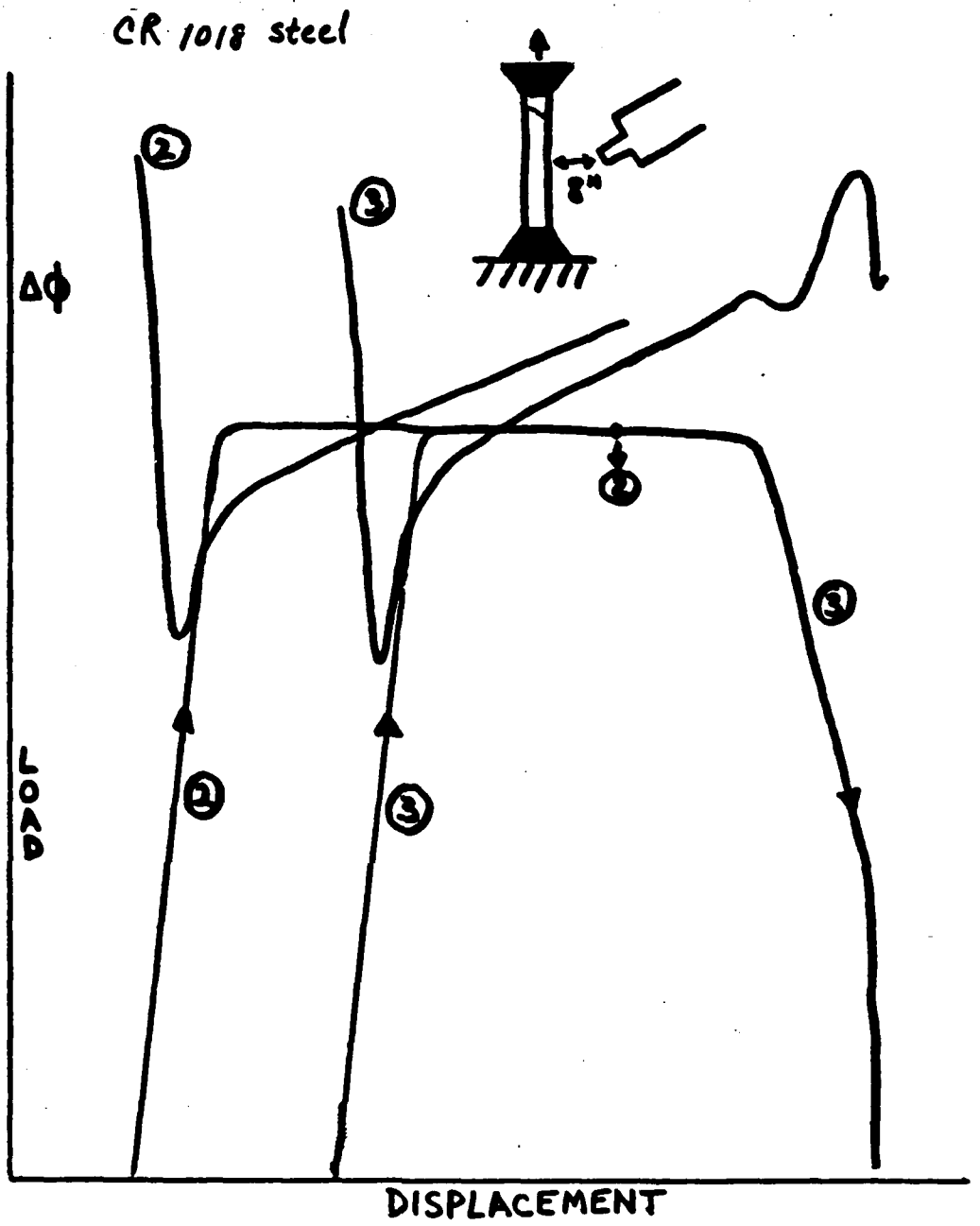
CR 1018 steel
2"
Δϕ
LOAD
DISPLACEMENT

LT-17 (Contributed Papers)
C. Ecker, A. Schmid, W. Weber, H. Wühl (eds)
© Elsevier Science Publishers B.V., 1984

SQUID DETECTION OF BARKHAUSEN THRESHOLD AND MAGNETIC KAISER EFFECT*

H. WEINSTOCK[+], T. ERBER[+], M. NISENOFF[++]

Illinois Institute of Technology[+] and U. S. Naval Research Laboratory[++]

A SQUID gradiometer placed in a residual field of less than 10^{-6} Oe has been used to measure the threshold of Barkhausen emission in a high purity, multicrystalline iron specimen. For low field excursions with $H \gtrsim 60$ mOe, magnetization reveals no further Barkhausen emission unless a previous maximum field value has been exceeded. This behavior (or magnetic Kaiser effect) continues until a second threshold at 158 mOe is reached. Beyond this point Barkhausen emission is observed on all increasing field cycles. Direct summation of the individual Barkhausen energy losses indicates that the total energy dissipated during the onset of hysteresis varies as $(H-H_t) + (H-H_t)^2$, where H_t is the field at which the first Barkhausen jump occurs.

1. INTRODUCTION

1.1. Background and motivation

Reversible magnetization changes in ferromagnets are usually attributed to reversible microstructural processes. At low fields the magnetization I and the field H are related by $\chi = I/H$. In iron χ is constant up to about 40 mOe. The complexities of the magnetization curve at higher fields, e.g., non-linearities and hysteresis, are often related to Barkhausen jumps: abrupt ($< 10^{-4}$s), irreversible shifts of the domain configurations.

The aim of the current work was to study the transition from reversible to irreversible behavior by using a SQUID gradiometer to determine whether there is a lower threshold for Barkhausen jumps. Another goal was to check whether Barkhausen emission could be diminished or eliminated by repe ted field cycling. If found, such behavior would be the magnetic analog of the Kaiser effect; this is a variation of acoustic emission that occurs during cyclic applied stress (1,2). Another aim of this work was to measure the energy losses associated with incipient hysteresis.

1.2. Equipment and sample

An S.H.E. Corporation SQUID (single axis) gradiometer was positioned at the center of an ultra-low field region provided by the 12.7 m diameter Braunbeck coil system at the Attitude Control Test Facility (ACTF) of the NASA-Goddard Spaceflight Center. Current up to 10 A, which could be ramped linearly with time, was applied to auxiliary coil windings to produce slowly varying, ambient fields from the null field of $H \leq 1$ μOe up to 367 mOe in either the axial (vertical) or a transverse (horizontal) direction to the SQUID gradiometer. Fields were applied in only one direction for a given set of runs.

The sample, composed of Johnson-Mathey 99.999% spectroscopically pure iron, was in the shape of a "pill" with a height of 2.67 mm and a diameter of 4.98 mm. This sample was demagnetized in the 10^{-6} Oe environment of the ACTF using a degaussing solenoid. After demagnetization, the pill, its axis collinear with that of the gradiometer coils, was centered just under the tip of the SQUID dewar. Other than this iron sample, no metallic objects were in the vicinity of the SQUID gradiometer coils.

This procedure yielded a pill magnetization of $\sim 6 \times 10^{-4}$ emu, in agreement with an estimate made for the practical lower limit for multi-domain samples. Additionally, peak-to-peak noise fluctuations due to the proximity of the pill were $\sim 4 \times 10^{-8}$ emu within a 0-10 Hz bandwidth, or about three times greater than those observed with no sample present.

2. RESULTS

2.1. Reversible magnetization

Upon applying a longitudinal ramping field at a uniform rate of 1.3 μOe/s up to 70 μOe, the magnetic moment of the sample changed linearly with field, achieving a maximum value of 6.0×10^{-7} emu. Ramping back to zero field produced a return to the original signal level to within an experimental precision of 2×10^{-8} emu. Additional field cycles up to 187 μOe produced the same I/H ratio and the same base signal upon removal of the ramping field.

These results show that the magnetization of this polycrystalline iron sample is reversible and devoid of Barkhausen jumps above a noise level of 3×10^{-8} emu.

2.2. Barkhausen threshold and magnetic Kaiser effect

A transverse field orientation was used in seeking the threshold of Barkhausen emission at higher fields. This orientation reduced the gradiometer response to sample magnetization by about two orders of magnitude without significantly degrading the response to randomly

* Supported in part by the Office of Naval Research and the Research Corporation.

oriented Barkhausen jumps.

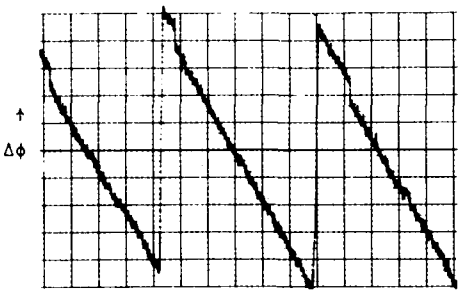

FIGURE 1

Figure 1 shows a typical gradiometer signal for an increasing field between about 230 and 310 mOe. Three Barkhausen jumps are clearly visible, i.e., well outside the range of instrumental noise.

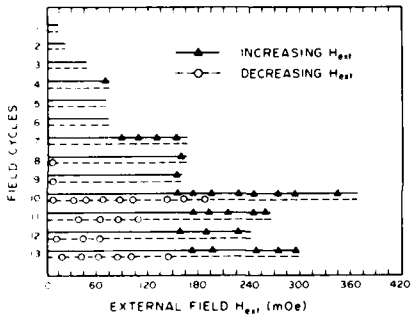

FIGURE 2

A summary of all Barkhausen jumps observed for the first 13 transverse field cycles is presented in Fig. 2. A complete analysis of Barkhausen emission observed for a total of 66 such cycles showed 82 jumps for 19 ascending fields and 52 jumps for the corresponding descending fields. Since all observed jumps are about an order of magnitude above the noise level, these observations do not support the notion of a smooth spectrum of jump heights gradually fading into the noise background.

One sees the first Barkhausen jump on run 4 at an ascending field of 68.9 mOe, but no jumps on runs 5 and 6 whose maximum fields just exceed 68.9 mOe. On run 7 one sees jumps for higher ascending fields, and again none for the descending sweep. Both runs 4 and 7 exhibit shifts between initial and final magnetizations commensurate with the change in magnetization due to Barkhausen jumps. The absence of jumps is the magnetic analog of the Kaiser effect.

Two additional phenomena can be observed in runs 8 to 13. First, one sees a threshold of persistent Barkhausen emission at increasing fields of about 158 mOe, i.e., subsequent runs to this or higher fields do not eliminate Barkhausen jumps at this value. Secondly, one sees jumps occurring at descending fields. Also, there is a 158 mOe field interval on any given run between the highest ascending field Barkhausen jump and the highest descending field jump. While this interval appears uniform, it is dependent on the maximum field reached. Detailed plots of the corresponding magnetization changes for successive runs exhibit a definite evolution from virgin to asymptotic behavior.

2.3. Hysteresis energy losses

The irreversible part of the energy change associated with change in magnetic moment is given as a discrete sum of the energy change associated with each Barkhausen jump. For each jump this energy is the product of the change in magnetic moment and the external field. Both the field and the corresponding change in magnetic moment were recorded for all Barkhausen jumps. The essential result of these measurements is that the energy losses could be represented by a formula of the type $(H-H_t) + (H-H_t)^2$, where H_t is the field at which the first Barkhausen jump occurred. Further analysis showed a linear behavior for the energy dissipation up to $(H-H_t) = 210$ mOe for 10 different runs. This "universal" linear behavior appears to result from two empirical regularities: (1) all jumps have the same order of magnitude; and (2) the field spacing between jumps is remarkably uniform.

Further work indicates that these phenomena are relevant to flux-jump behavior, i.e., training, in superconducting magnets and in simplifying the analysis of energy losses in superconducting systems.

ACKNOWLEDGEMENTS

The authors wish to thank Drs. Mark Rubinstein and Peter Lubitz of the Naval Research Laboratory for supplying the sample and their helpful advice, and Messrs. Chuck Harris and Bob Bender of the NASA-Goddard Spaceflight Center for helping one of us (H.W.) with the measurements.

REFERENCES

(1) J. Kaiser, Arch. Eisenhüttenwesen 24 (1953) 43.
(2) G. Pasztor and C. Schmidt, J. Appl. Phys. 49 (1978) 886.

Threshold of Barkhausen emission and onset of hysteresis in iron

H. Weinstock* and T. Erber†
Department of Physics, Illinois Institute of Technology, Chicago, Illinois 60616

M. Nisenoff
Naval Research Laboratory, Washington, D.C. 20375

(Received 1 June 1984)

The threshold of Barkhausen emission and hysteresis in a polycrystalline sample of iron has been measured using a SQUID (superconducting quantum-interference device) magnetic gradiometer in a residual field of less than 10^{-6} Oe. In the range $10^{-6} \leq H \lesssim 2\times 10^{-4}$ Oe, the magnetization was found to be proportional to the applied field and varied reversibly without any discernible Barkhausen emission greater than 10^{-8} emu. At higher field levels, the appearance of isolated Barkhausen jumps coincided with the onset of magnetic hysteresis. Repeated field cycles in this threshold region removed the Barkhausen signals and extended the range of reversible magnetization (equivalent to a magnetic Kaiser effect). At still higher field levels, a second threshold of nonvanishing Barkhausen emission and hysteresis appeared. Direct summation of the individual Barkhausen energy losses indicates that the total energy dissipated during the onset of hysteresis varies as $(H-H_t)+(H-H_t)^2$, where H_t is the field at which the first Barkhausen jump occurs. Measurements also were made on a single-crystal iron whisker. At higher field levels, occasional Barkhausen emission was observed, but in most instances the data showed irreversible behavior without observable Barkhausen discontinuities. The observations for both the multicrystalline and single-crystal specimen are found to be consistent with the consequences of a general phenomenology of hysteresis.

I. INTRODUCTION

A. Reversible and irreversible magnetization processes

The availability of SQUID (superconducting quantum-interference device) magnetometers capable of detecting flux variations of the order 10^{-17} Wb, or 10^{-9} Mx, has made it feasible to investigate the transition from reversible to irreversible behavior in the magnetization of ferromagnetic materials. Experiments carried out in an ultra low-field environment (10^{-6} Oe over a volume of 20 m^3), with superposed uniform fields swept at rates as slow as 10^{-6} Oe/sec, have shown that in polycrystalline iron there is a sharp demarcation between reversible and irreversible magnetization. The appearance of isolated Barkhausen jumps coincides precisely with the onset of hysteresis. Furthermore, the net changes in magnetization resulting from external-field cycles correspond approximately to the algebraic sums of the intervening Barkhausen jumps.

Before discussing these observations in detail, it is useful to provide some background on ferromagnetism in weak magnetic fields. The basic processes underlying reversible magnetization changes in ferromagnets are usually identified with reversible domain-wall bowings or displacements, and reversible rotations of the magnetizations of individual domains.[1,2] The experimental information concerning reversible-magnetization changes in macroscopic ferromagnet may be summarized as follows:[3] If H is the magnetic field and I is the corresponding magnetization, then

$$I = \chi H \ , \tag{1.1}$$

where the susceptibility χ is strictly constant for arbitrary variations of H in the range

$$0 < H_L \leq H \leq H_U \ll H_C \ . \tag{1.2}$$

Here, H_C is the coercive field, which for iron is on the order of 0.1—5 Oe, depending on sample purity and preparation. In practice, the upper limit of reversible magnetization for iron is approximately $H_U \sim 0.04$ Oe, while the lower bound, H_L, is limited by thermal fluctuations[4,5] (see Sec. III A). Rayleigh estimated that $H_L \sim 10^{-5}$ Oe,[6] but more recent measurements on nickel ellipsoids—shielded from stray external fields exceeding 10^{-5} Oe—showed irregular variations of I for fields below $H_L \sim 10^{-3}$ Oe[7,8]

The simplest reproducible results for irreversible magnetization changes in ferromagnets are also obtained in weak magnetic fields. In contrast to Eq. (1.2), the fields are first increased along the virgin curve to some maximum value H_m,

$$0 \rightarrow H \rightarrow H_m \ , \tag{1.3}$$

and then symmetrically cycled between the limits

$$H_m \rightarrow H \rightarrow 0 \rightarrow -H \rightarrow -H_m \quad \text{(descending)} \tag{1.4a}$$

and

$$-H_m \rightarrow -H \rightarrow 0 \rightarrow H \rightarrow H_m \quad \text{(ascending)} \ . \tag{1.4b}$$

After a few cycles the magnetization is described by the well-known Rayleigh law[6]

$$I(H) = (\chi_4 + \alpha H_m)H + \tfrac{1}{2}\alpha(H_m^2 - H^2) \ , \tag{1.5}$$

where the upper and lower signs correspond to the descending and ascending branches, respectively. For unannealed iron, typical values for the parameters are χ_A (initial susceptibility) ~ 7, and α (Rayleigh constant) ~ 4, when H is measured in Oe.

These irreversible—albeit reproducible—variations of $I(H)$ are observed only over a limited range of the maximum field H_m. If the bounds of this "Rayleigh region" are denoted by H_L^R and H_U^R, then H_m is restricted by a set of inequalities analogous to Eq. (1.2),

$$0 < H_L^R \leq H_m \leq H_U^R < H_C \ , \tag{1.6}$$

where H_C is again the coercive field. Representative values of H_U^R are 1.4 Oe (for "hard" Swedish iron[6]), 3.2 Oe (for "powdered" iron[9]), and 0.38 Oe (for annealed iron[10]). Ellwood also verified the existence of well-defined hysteresis loops of the type [Eq. (1.5)] for field excursions as small as $H_L^R \simeq 55.8$ mOe.[9] Even lower values, $H_L^R \sim 5$ mOe, have been obtained with window-frame monocrystals of Fe-Si.[11] For later reference, we note that the remanence, which is a measure of the nonuniqueness of I, is given by

$$I_R = \tfrac{1}{2}[I(H=0 \text{ , descending branch}) - I(H=0 \text{ , ascending branch})] \ , \tag{1.7}$$

where, by virtue of Eq. (1.5),

$$I_R = \tfrac{1}{2}\alpha H_m^2 \ . \tag{1.8}$$

In Ellwood's work,[9] $I_R = 10^{-4}$ Oe, with $H_m \sim 55.8$ mOe and $\alpha \sim 0.064$.

Irreversible magnetization changes are usually attributed to Barkhausen jumps.[12,13] These discontinuities are produced by abrupt ($< 10^{-4}$ sec) shifts in domain configurations caused by the movement of walls. It is assumed that dislocations, precipitates, or other obstacles normally pin the walls, but if external fields exceeding certain threshold values are applied, then the walls are able to surmount these potential barriers and move until they are snagged by the next potential peaks.[14] This situation is indicated schematically in Fig. 6(a)—also see Sec. IV. A statistical treatment of random jumps over this "landscape" of potential hills and valleys leads to a polynomial expansion for the magnetization,[15]

$$I(H) = aH + bH^2 + \cdots \ . \tag{1.9}$$

Experiments confirm that this type of quadratic expression fits the virgin magnetization curve. However, since the statistical arguments are applied to a *fixed* landscape of microscopic potential curves, it is not possible to account for the evolution of virgin to asymptotic hysteresis.

B. Open problems

1. Discordant experiments

In this brief treatment of weak-field ferromagnetism we have already mentioned experiments that indicate a failure of the simple proportionality in Eq. (1.1) for extremely weak fields.[7,8] The discrepancies associated with irreversible magnetization are far more serious and well documented: First, we recall that the measurements carried out by Ellwood were intended to settle a long-standing controversy concerning hysteresis losses in the Rayleigh region.[9] From Warburg's principle (cf. the Appendix) it follows that the energy dissipated per cycle over a Rayleigh loop is given by

$$W_R = \tfrac{4}{3}\alpha H_m^3 \ . \tag{1.10}$$

However, early experiments by Jordan[16] and Gans[17] showed that the energy losses included a *quadratic* term:

$$W_{JG} \propto H_m^2 + H_m^3 \ . \tag{1.11}$$

Ellwood's attempts to resolve this discrepancy were ambiguous: on one hand, his results confirmed that the *areas* of the Rayleigh loops were strictly proportional to H_m^3, but direct ac-bridge measurements of the power dissipation also showed that the magnetic hysteresis losses were described by the Jordan-Gans form, Eq. (1.11). In particular, for fields in the range $0.05 \lesssim H_m < 0.4$ Oe, the evidence was clear that the energy losses varied as $W \propto H_m^2$.

Forty years later, similar results were obtained by Baldwin.[18,19] Using updated bridge methods he verified that Ni-Fe and several gadolinium samples exhibited standard Rayleigh hysteresis in weak fields (for Gd, $0.02 \lesssim H_m \lesssim 0.6$ Oe), but at still lower field levels (0.1—10 mOe) all the samples showed a transition to the quadratic Jordan-Gans type of energy dissipation. Baldwin emphasized that series expansions such as Eq. (1.9) were bound to lead to quadratic and cubic variations for the remanence and energy losses and could not be reconciled with the results of the low-field measurements.

2. Too many Barkhausen jumps

When the amplitude of the magnetic field sweeps is decreased below H_U^R, as defined in Eq. (1.6), there is a rapid decrease in the number of Barkhausen jumps.[10,12,20] There is an isolated claim that below a certain threshold they disappear altogether,[21] but the prevailing opinion is that smaller fields are generally associated with smaller jumps.[11] This makes it plausible that the smooth variation of the magnetization at the lowest field levels is simply an artifact of limited experimental resolution. At the domain level this implies that reversible and irreversible wall deformations always coexist, and that the magnitude of the applied field simply varies the mix. Since a linear relation such as Eq. (1.1) is incompatible with hysteresis, the ultimate conclusion of this line of reasoning is that the linear Rayleigh law is simply an empirical approximation without deeper significance.

3. Too few Barkhausen jumps

It is curious that the same arguments that cast doubt on the validity of Eq. (1.1) also may be turned against the other Rayleigh law, Eq. (1.5). The essential point is that if irreversible magnetization is actually the cumulative result of statistical wanderings over a microscopic energy landscape, then sensitive detectors should show that the two branches of the Rayleigh loop are, in fact, generated by distinct patterns of Barkhausen jumps. This assertion has been checked experimentally by Bush and Tebble,[22]

TABLE I. Contributions of discontinuous and reversible processes to the total change in magnetization.

Material	Barkhausen magnetization I_{irr} (%)	Reversible magnetization I_{rev} (%)	Missing magnetization $I_T - I_{irr} - I_{rev}$ (%)	Barkhausen energy / Hysteresis loop energy
Hard-drawn iron[a]	86	9	5	
Large-grained iron[a]	57	5	38	
Nickel[a] (annealed)	47	16	37	
Nickel[b] (hard)	<20			<0.2

[a]Reference 23.
[b]Reference 24.

and Tebble, Skidmore, and Corner,[23] at Leeds; and also by Koller, Pfrenger, and Stierstadt[24] at Munich. For hard-drawn iron, the Leeds group obtained consistent results. As shown in Table I, the total change in magnetization (I_T) measured for a half-cycle of a stabilized hysteresis loop was nearly equal to the sum of discontinuous magnetization changes due to Barkhausen jumps (I_{irr}) and a small reversible component (I_{rev}). However, for large-grained iron and annealed nickel, about 40% of the total magnetization changes could not be accounted for by experimentally integrating along the hysteresis loop. The last line of Table I summarizes the results of Koller *et al.*: Both in hard and soft nickel samples, the discontinuous magnetization changes were far too small to explain the observed hysteresis. Moreover, the energy dissipated in irreversible jumps was less than 20% of the energy losses inferred from the areas of the hysteresis loops. The only possible way of reconciling these results with statistical hysteresis theories, such as Néel's,[15] is to suppose that there are very many Barkhausen jumps that are so small that they fall below the threshold of experimental resolution.

4. *Barkhausen jumps and the magnetic Kaiser effect*

It is apparent from Eqs. (1.2) and (1.6) that reversible and irreversible magnetization changes can occur at the same field levels, for instance, in iron at 40 mOe. This does not imply any inconsistency: As indicated in Eqs. (1.4a) and (1.4b), the virgin curve will split progressively into Rayleigh loops when the field cycles include changes in direction, i.e., *two-sided hysteresis.* On the other hand, if the field varies in magnitude but not in direction, then the linear behavior of Eq. (1.1) persists. In fact, experiments support a stronger claim: If, in the case of iron, one starts at a base field of 0.4 Oe$\simeq 10H_U$ [cf. Eq. (1.2)] and then applies symmetric field cycles with amplitudes bounded by H_U, i.e., *one-sided hysteresis,* then the hysteresis implicit in Néel's expansion, Eq. (1.9), *disappears,* and the susceptibility in the range $10H_U \pm H_U$ becomes strictly constant.[6] The I_{rev} entries in column 3 of Table I were obtained essentially by this method.[3,23]

Since one-sided hysteresis cycles can create localized intervals of constant, or reversible, susceptibility, it is plausible to assume that the intensity of Barkhausen emission in these intervals should also decrease or disappear altogether. Specifically, starting from a given base field, the irreversible magnetization and Barkhausen emission on the *first* field increase above the base level should be greater than the corresponding changes on subsequent cycles. Such a progressive quenching of Barkhausen emission in one-sided hysteresis would be a magnetic counterpart of the Kaiser effect in acoustic emission.[25–27] Both effects are consequences of a general hysteresis theory—see Sec. IV.

C. Scope of the present work

This background of open problems and conjectures suggested a series of experiments intended to answer the following specific questions:

(a) Is there a definite lower threshold for the Barkhausen effect? In other words, is there a very-low-field regime where the magnetization is uniquely determined by the field?

(b) Is the onset of the Barkhausen effect always correlated with the appearance of hysteresis? Can the total changes in magnetization be accounted for by summing the reversible components and the Barkhausen jumps?

(c) Is it possible to diminish or eliminate Barkhausen emission by repeated field cycles? Is there a magnetic Kaiser effect?

(d) What are the energy losses for incipient hysteresis? How can Warburg's principle be modified for open or drifting hysteresis loops?

(e) Are there any indications that it is possible to have multivalued, i.e., history-dependent, magnetization without any apparent Barkhausen jumps?

The results of the present work are summarized in Sec. V.

II. EQUIPMENT AND SAMPLES

A. Magnetic gradiometer

A S.H.E. Corporation model BMP SQUID biomagnetic gradiometer was used to measure the magnetization of several pure iron samples in an ultralow-field environment provided by the NASA Goddard Space Flight Center Attitude Control Test Facility at Greenbelt, Maryland (NASA denotes National Aeronautics and Space Administration). The overall setup of the experiment is shown in Fig. 1. The gradiometer coil is 6.3 cm long and 2.3 cm in diameter; its axis was positioned vertically for all measurements. This coil had a total of eight turns: the two turns at the top and the two at the bottom were wound in the same direction, while the four turns in the middle

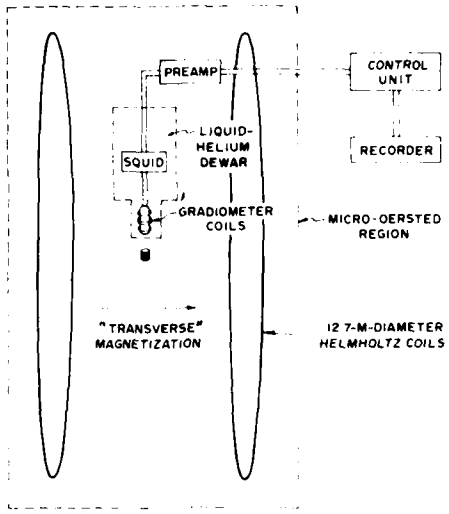

FIG. 1. Schematic of SQUID setup at the NASA Attitude Control Test Facility. A three-axis, 12.7-m-diam Braunbeck coil system provides a cancellation of the geomagnetic field to $\pm 10^{-6}$ Oe over a volume of 20 m^3.

were wound in the opposite direction. This configuration produces a null output voltage in the presence of a uniform magnetic field or a field with a constant gradient, i.e., it is a second-derivative gradiometer. When this coil arrangement is placed inside a helium Dewar, the bottom two turns are approximately 1.0 cm above the bottom outside surface of the Dewar. If a small ferromagnetic sample is placed in the vicinity of the Dewar bottom, its magnetization is sensed principally by the lower two turns of the SQUID coils. If the magnetization is altered by means of a *uniform* external field, as indicated in Fig. 1, then the gradiometer will sense only the changes in magnetization of the sample. It is important to note that a SQUID-based gradiometer has a dc response. Thus, it measures magnetic moment or flux directly, whereas most other types of magnetometry involve the time derivative of these quantities.

Leads from the gradiometer coils are connected to the input terminals of the S.H.E. Corporation Hybrid™ SQUID Sensor. The sum of instrumental and environmental noise in the (0—10)-Hz bandwidth was on the order of 4×10^{-10} G/$Hz^{1/2}$. Under these operating conditions, the limiting slew rate of the SQUID is $10^5\Phi_0$/sec, where $\Phi_0 = hc/2e = 2.07\times10^{-7}$ G cm^2.

The SQUID calibration was checked by a simulation of the magnetization experiments. A five-turn test coil with an overall length of 3 mm and a 28.3 mm^2 cross section was fabricated. These dimensions approximated the iron sample used in most experiments. The test coil was placed at several distances below the Dewar tail along the axis of the gradiometer, and the change in SQUID output as a function of dc current in the test coil was determined. In a range of the sample positions from 1 to 15 mm below the Dewar bottom, the test-coil results and the quoted SQUID-calibration value agreed to within 10%.

B. Magnetic field facility

All magnetization measurements were carried out at the Attitude Control Test Facility (ACTF) of the NASA Goddard Space Flight Center at Greenbelt, Maryland. The ACTF building is a nonmagnetic cement-block structure containing a three-axis 12.7-m-diam Braunbeck coil system that can compensate for various kinds of field inhomogeneities such as diurnal variations, temperature-induced gradients, etc. This arrangement provides an overall cancellation of the geomagnetic field to within $\pm10^{-6}$ Oe, and a field homogeneity of 0.001% over a spherical volume of 24.4 m^3.

Auxiliary windings in the Braunbeck coil system were used to generate uniform magnetizing fields, as shown in Fig. 1. The currents in these windings were derived from two operational amplifiers whose output voltages could be ramped linearly in time for durations between one second and several thousand seconds. The output from this circuit drove a Hewlett-Packard model 6269B dc power supply operated in a voltage-programmable amplifier mode. This power supply is capable of delivering a 40-V output with a 20-A drain. However, the ACTF coil sets, when connected in parallel, presented a net resistance of 4 Ω, thereby limiting the attainable current to about 10 A. The corresponding peak magnetic fields at the sample position were limited to 0.37 Oe (see run 10 in Fig. 3). This arrangement permitted field-sweep rates as slow as 0.81 μOe/sec. The magnetic fields at the samples could be raised to still higher levels by combining this variable-field arrangement with fixed base fields. For this purpose other auxiliary windings in the Braunbeck system could provide dc fields in steps of 1×10^{-6} Oe up to a maximum of 0.6 Oe.

When the gradiometer coils were centered within the Braunbeck coil system, the SQUID could be balanced to about one part in 10^6 for the north-south and east-west directions, and to about one part in 10^5 for the vertical direction. The response of the SQUID (without any sample present) to a ramped field in any of these directions was then due to residual imbalances in the gradiometer and spatial nonuniformities of the ramping field. In general, the SQUID response to a ramped field in the absence of any sample was never more than a few percent of the response observed when one of the iron samples was positioned within 2 or 3 cm of the Dewar bottom.

C. Iron samples and demagnetization procedures

The combination of the ACTF environment and SQUID magnetometer was used to spot-check the magnetization of a variety of samples including gadolinium and a metallic glass ribbon. However, the detailed studies described in the next section were carried out on two iron samples. One of these, which we shall refer to as the "pill," was cut from a circular rod of Johnson-Mathey 99.999% spectroscopically pure iron. This sample was annealed in a hydrogen atmosphere at 650°C for several hours. The average height of the sample was 2.67 mm and its diameter was 4.98 mm, or approximately the size of a pill. This sample weighed 0.406 g and had a computed volume of 5.20×10^{-2} cm^3; these values are consistent with the handbook density of 7.874 g/cm^3 for pure Fe. The other sample is an iron whisker 1.72 cm long with an average rectangular cross section of 0.14 mm^2, kindly pro-

vided by Professor R. V. Coleman of the University of Virginia. This whisker was also annealed prior to the experiments.

All samples were carefully demagnetized in the 10^{-6} Oe environment of the ACTF immediately before the measurements. Two variac voltage dividers in series were connected to a small degaussing solenoid that could generate a field of 2 kOe with the full 110-V ac line voltage across it. With a sample placed inside the solenoid, the (secondary) variac connected directly to the demagnetizing solenoid was adjusted to its maximum voltage setting of 130 V. The primary variac was initially set to a high value, usually about 90 V, so that the current through the solenoid was just less than 20 A. The primary variac setting was then reduced at a decreasing rate during a period of a few minutes until a value of 1–2 V was reached. The secondary variac was then turned down in a similar fashion, also stopping at a setting of 1–2 V. Owing to the series variac arrangement, this final setting corresponded to 10^{-2} V. The sample was then withdrawn slowly and placed on a platform directly under the SQUID Dewar. The demagnetizing solenoid was also slowly moved to a location far from the field-free ACTF region before the remaining current was disconnected. Apart from the iron samples, no ferromagnetic objects were anywhere near the SQUID gradiometer coils.

The domain structure of ferromagnetic samples sets a practical lower limit on all demagnetizing procedures. Studies of erasure limits and noise on tape recordings indicate that, to a good approximation, the lower limits of magnetization ($|I|_{\text{demag}}$) can be estimated by adding the magnetic moments of individual domains ($\vec{m}_{\text{dom}}$) by "random-walk" methods, i.e.,

$$|I|_{\text{demag}} \sim \frac{1}{V}\left\langle\left|\sum \vec{m}_{\text{dom}}\right|\right\rangle \sim \frac{1}{V}\left(\frac{8n}{3\pi}\right)^{1/2}|\vec{m}|_{\text{dom}}\,, \quad (2.1)$$

where n is the number of domains in the sample and V is the sample volume. By this means one can crudely estimate that, for the pill, $10^{-4} \lesssim |I|_{\text{demag}} \lesssim 10^{-3}$ emu, and, indeed, after demagnetization, the SQUID signals indicated a residual magnetization on the order of 6×10^{-4} emu.

At the end of their long article on the Barkhausen effect, Tebble *et al.*[23] recommend that future work be done with samples having large demagnetizing factors. This criterion has been met in the dimensions chosen for the pill sample. Large demagnetizing factors are helpful in avoiding clusters or avalanches of Barkhausen jumps. This becomes clear if we recall that the effective magnetic field inside a sample (H_{int}) is related to the applied field (H_{ext}) by

$$H_{\text{int}} = H_{\text{ext}} - NI\,, \quad (2.2)$$

where N is the demagnetizing factor. Assuming, as usual, that the magnetization is [cf. Eq. (1.1)]

$$I = \chi H_{\text{int}}\,, \quad (2.3)$$

then Eq. (2.2) indicates that the internal field is given by

$$H_{\text{int}} = H_{\text{ext}}/(1+N\chi)\,, \quad (2.4)$$

and, furthermore, that

$$I = \frac{\chi}{1+N\chi}H_{\text{ext}} \sim H_{\text{ext}}/N \quad \text{when } N\chi \gg 1\,. \quad (2.5)$$

The pill's "longitudinal" demagnetizing factor for fields parallel to the 2.67-mm axis is $N_l \simeq 5.6$—see Eq. (3.1) *et seq.* In addition, for pure iron, the initial susceptibilities are in the range $20 \lesssim \chi \lesssim 80$. According to Eq. (2.4) the internal fields in the pill are then at least a factor of 100 smaller than the applied fields. With external field-sweep rates of 10^{-6} Oe/sec and an instrumental resolution of 0.1 sec, it should, in principle, be possible to discriminate Barkhausen jumps separated by only 10^{-9} Oe. For samples at room temperature, such small field increments are probably comparable to fluctuations induced by thermal noise.[4,14]

III. EXPERIMENTS

A. Reversible magnetization

The iron pill sample described in Sec. II C was demagnetized and placed against the bottom of the Dewar. The residual magnetic moment was measured to be about 2×10^{-5} emu, cf. Eq. (2.1). In the most sensitive range, there was a signal with a peak-to-peak value of 4.2×10^{-8} emu in the bandwidth from 0 to 10 Hz. These fluctuations were roughly a factor of 3 greater than those observed in the absence of any samples. It was not determined whether these fluctuations were due to mechanical vibrations or thermal noise. Next, a uniform vertical field, i.e., one aligned with the gradiometer axis and the 2.67-mm axis of the sample, was applied. This field was first increased from (0 ± 1) to (70 ± 1) μOe at a uniform rate of 1.3 μOe/sec, and then uniformly decreased to (0 ± 1) μOe. This cycle was repeated once again. The magnetic moment of the sample changed by 6.0×10^{-7} emu as the field was increased from 0 to 70 μOe. The net change in magnetic moment over a complete cycle ($0\rightarrow70\rightarrow0$ μOe) was less than 2×10^{-8} emu.

It is clear from all low-field traces that apart from a fluctuating component, the magnetization is strictly proportional to the applied field and completely reversible. These results can also be checked with the help of Eq. (2.5). Inserting the experimental values, we find

$$\frac{I}{H_{\text{ext}}} = \frac{1.16\times10^{-5}\text{ emu}}{7.0\times10^{-5}\text{ Oe}} \cong 0.166 \cong N_l^{-1}\,, \quad (3.1)$$

where N_l is the longitudinal demagnetizing factor. An independent measurement of the demagnetizing factors of the pill carried out with a PAR model 150 vibrating-sample magnetometer yielded a value of $N_l^{-1}=0.178$. Both of these results are in good agreement with the semi-itheoretical estimate (based on sample dimensions) $N_l^{-1}=0.177$ given by Warmuth.[29] Similar results were obtained with additional field cycles extending to 187 μOe.

The questions raised in item (a) in Sec. I C can now be answered as follows: For very slow field sweeps in the range 1–187 μOe, the magnetization in a polycrystalline sample of pure iron is reversible and without any Barkhausen jumps above a noise level of about 3×10^{-8} emu. Owing to the large demagnetizing factor of this sample, the corresponding internal fields are lower by a

factor of $(1-4)\times 10^2$, cf. Eq. (2.4). Since $N\chi \gg 1$, it is clear from Eq. (2.5) that the ratio I/H_{ext} is insensitive to the magnitude and any possible dependence of χ on applied field.

B. Threshold of Barkhausen emission: The magnetic Kaiser effect

1. *Barkhausen signals*

The magnetization measurements of the iron pill sample were gradually extended to higher transverse field levels until finally isolated jumps of the type shown in Fig. 2 appeared. Since the noise fluctuations are symmetrically distributed about the linear rise in magnetization, these asymmetric shifts stand out conspicuously. A typical jump corresponds to a change in magnetic moment of 5×10^{-8} emu; this value is about an order of magnitude smaller than the jumps reported by Tebble *et al.*,[23] but quite reasonable for Barkhausen signals. These magnetic-moment changes, of course, correspond to abrupt shifts in the *total* magnetization of the pill. The connection between bulk magnetization changes and localized rearrangements of the domain structure can be established only by means of model-dependent boundary-value problems.[30]

The intrinsic switching time for Barkhausen jumps is controlled by domain-wall movements.[12] Since the wall velocities are of the order of 10^3-10^5 cm/sec, the corresponding jump durations may be as short as 10^{-6} sec. However, if the Barkhausen jumps occur in the interior of a conducting material, the corresponding magnetization of the bulk sample will switch on a slower time scale because of eddy-current decays. In particular, for an infinitely long cylinder with permeability μ and conductivity σ, the effective eddy-current-decay time is[31]

$$\tau \sim \pi\mu\sigma a^2 , \tag{3.2}$$

where a is the radius of the cylinder. Assuming $\mu \sim 400$, $\sigma^{-1} \sim 10^{-5}\ \Omega$ cm, and $a \simeq 2.4$ mm, Eq. (3.2) indicates that the magnetization of the iron pill will switch on a time scale of about $\sim 4\times 10^{-3}$ sec. If we combine this estimate with the maximum slewing rate of the SQUID gradiometer ($\sim 10^5 \Phi_0$/sec) for this frequency domain, we find an upper limit on the order of 10^{-5} emu for the magnetic moments of the Barkhausen jumps that can be measured when the pill is placed within 1–2 cm of the Dewar bottom.

The slowest element of our analyzing system was a strip-chart recorder with an effective bandwidth of 10 Hz. This affected our ability to detect Barkhausen jumps at higher field levels and faster sweep rates. Consider, for example, the situation where the pill is placed against the Dewar bottom and a vertical field is applied as in Sec. III A. In this case, Eq. (3.1) implies that

$$\frac{\Delta m_p}{\Delta H_{\text{ext}}} = \frac{6.0\times 10^{-7}\ \text{emu}}{70\ \mu\text{Oe}} \sim 0.86\times 10^{-8}\ \text{emu}/\mu\text{Oe} , \tag{3.3}$$

where Δm_p is the change in the magnetic moment of the pill. If the field is swept at a rate of 1.3 μOe/sec, then in 0.1 sec the *continuous* change in moment is $\sim 10^{-9}$ emu, whereas the discontinuous change due to a Barkhausen jump is $\sim 5\times 10^{-8}$ emu. This disparity is the reason that the Barkhausen jumps stand out so clearly in the traces shown on Fig. 2. However, these estimates also make it clear that with faster sweep rates, say 300–500 μOe/sec, the Barkhausen discontinuities will no longer be visible as steps on the strip-chart traces. This problem can be avoided with oscilloscope recording and/or compensating coils, but with the means at hand it was decided to use transverse magnetization to enhance the Barkhausen signals. The transverse-field orientation is shown in Fig. 1.

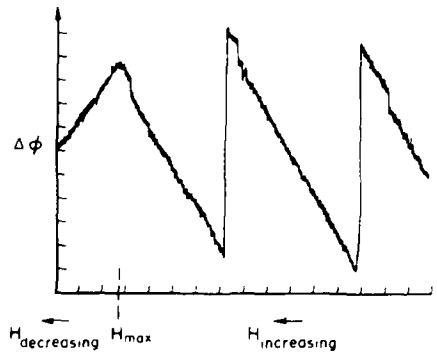

FIG. 2. Strip-chart record of changing flux (on the vertical scale) as a function of external field (on the horizontal scale) showing three Barkhausen jumps near the peak field on run no. 13. The jumps are equivalent to magnetic-moment changes of $\sim 10^{-7}$ emu in the iron pill sample. The field was ramped at 0.897 mOe/sec. The two full-scale vertical lines are due to manual resets. The peak field, seen near the left end of the figure, was 299 mOe.

All the Barkhausen measurements reported in this section were obtained with this transverse-field orientation. As indicated in Sec. II B, ramping auxiliary field coils in the transverse direction produced no significant imbalance in the gradiometer response unless an iron sample was present. The essential point of this arrangement is that if the magnetized sample is represented by a finite solenoid, then in the transverse orientation the coupling between the magnetization of the sample and the gradiometer coil system can be minimized. Allowing for slight asymmetries in the geometry of the iron pill, angular misalignments of 1°–2°, and centering errors of 0.1–0.2 mm, it is easy to show that the gradiometer response to the sample magnetization is reduced by about 2 orders of magnitude. Since the transverse demagnetization factor of the sample is approximately $N_t = 3.6$, as determined by independent measurements, this reduction also could be verified experimentally. However, the gradiometer coupling to randomly oriented Barkhausen jumps was not affected by this choice of field direction.

All of the information concerning Barkhausen emission displayed in Fig. 3 was obtained with the iron pill positioned so that there was a 1.18-cm gap between its top surface and the Dewar bottom, and with the field in the transverse orientation. Under these conditions the slope of the *continuous* portion of the magnetization curve cor-

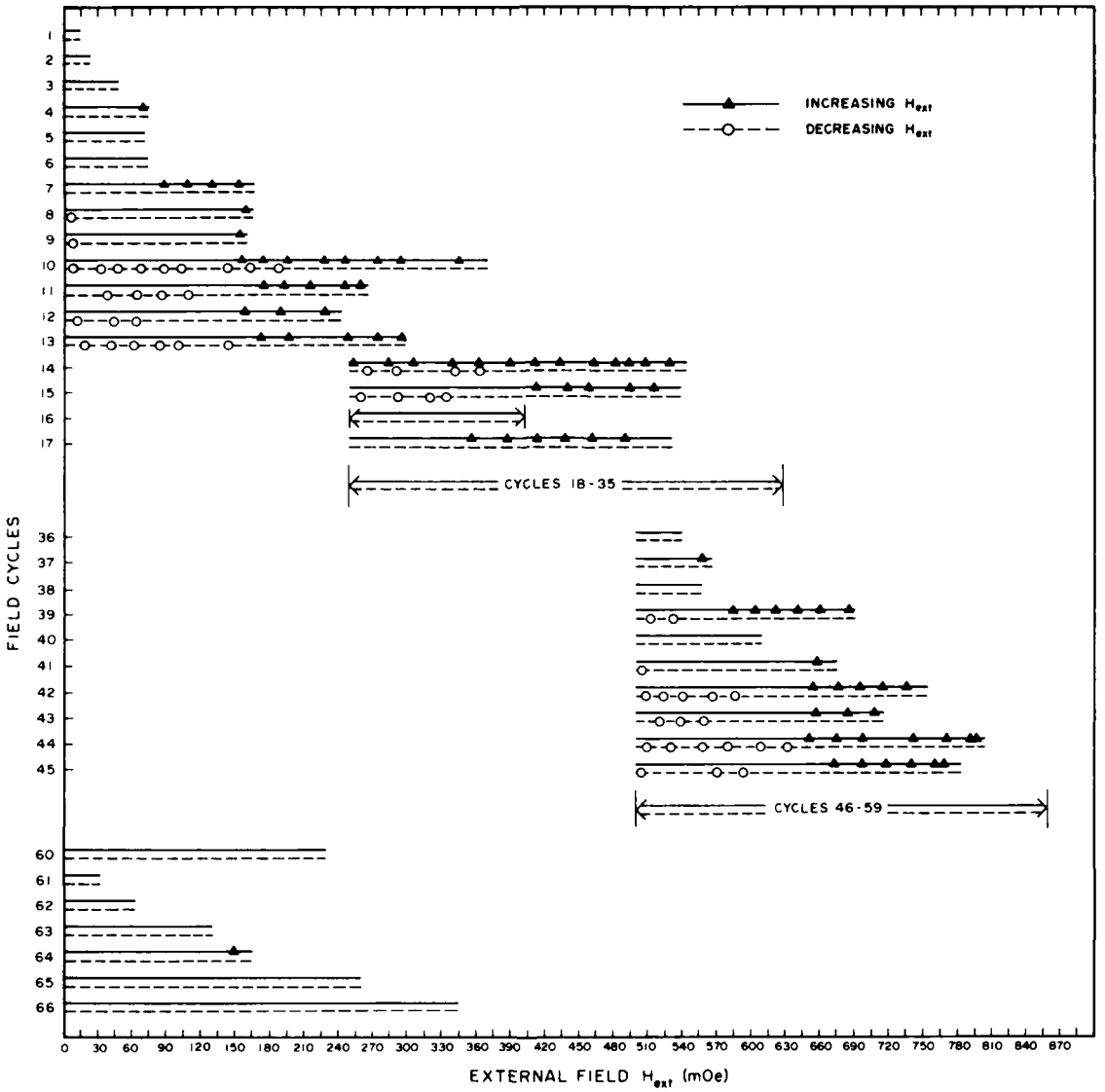

FIG. 3. Pattern of Barkhausen jumps for a polycrystalline iron sample. The solid triangles indicate the fields where jumps occurred during increasing field sweeps; the open circles show the jumps observed on decreasing field sweeps. Spurious signals occurred during run no. 16 and the down-field part of run no. 17.

responded to SQUID signals of approximately $181\Phi_0$/Oe. Allowing for *maximum* sweep rates of 900μOe/sec, this resulted in increments of $0.0163\Phi_0$ in 0.1 sec. In contrast, typical Barkhausen discontinuities corresponded to shifts of about $0.3\Phi_0$.

2. *Threshold of Barkhausen emission*

As indicated in Fig. 3 the first Barkhausen jump occurred at $H_{ext} = 68.9$ mOe on run no. 4. The magnitude of the change in magnetic moment was $\Delta m_B = 1.57 \times 10^{-7}$ emu with a $\pm 10\%$ error. According to Eq. (2.4), because of the demagnetizing effect, the internal field in the sample is lower by a factor of roughly $(1-4) \times 10^{-2}$. Strictly speaking, the onset of Barkhausen emission may mark the end of a gap rather than a threshold because on the prior lower-field runs (nos. 1–3) Barkhausen jumps might have occurred below the noise level of 3×10^{-8} emu. Nevertheless, the present observations exclude the possibility that there is a smooth spectrum of Barkhausen signals gradually fading below the noise level. The existence of a gap, or terminus, in the Barkhausen spectrum is dependent on the nature of the sample as well as on the method of magnetization: A cursory check of a (metastable) metallic glass sample showed an extremely high level of spontaneous Barkhausen noise in a zero-field environment. On the other hand, it is known that high demagnetizing factors and transverse magnetization inhibit Barkhausen emission.[12,31]

The existence of a threshold in Barkhausen emission also was checked in another series of runs with the pill sample placed against the gradiometer Dewar. The observed pattern was entirely analogous to that shown in run nos. 1–4 in Fig. 3, except that the initial jump occurred at a lower field level, $H_{ext} = 48.8$ mOe.

It also is apparent from Fig. 3 that when the field on run no. 4 was decreased from its maximum value of 74.7 mOe there were no further Barkhausen jumps. A com-

parison of the initial and final magnetization of the sample showed that the difference was completely accounted for by the single Barkhausen event. The slopes of the ascending and descending magnetization records were equal within experimental error.

3. *Magnetic Kaiser effect*

The one-sided hysteresis cycles shown in Fig. 3 include 82 Barkhausen jumps on 19 ascending branches and 52 jumps on the corresponding descending branches. In addition to this obvious division, there are definite patterns in the distribution of the jumps. It is clear from cycle nos. 4–8, 37–40, and 60–66 that the Barkhausen jumps appear on the *first* field sweeps to higher levels, and in subsequent cycles the jumps reappear only for field values exceeding the peak fields reached in the preceding sweeps. Similar "memory" effects in Barkhausen emission have been observed in polycrystalline gadolinium when subjected to field cycles of increasing amplitude in the range 2–18 Oe.[32] The first example of such a regime of disappearing discontinuities was found by Kaiser in acoustic emission.[25–27]

In all the cycles shown in Fig. 3, it was possible to check the magnetization changes explicitly (cf. Table II). In every case the net magnetization change over a complete field cycle was commensurate with the cumulative increments of the Barkhausen jumps. In this sense the onset of hysteresis and Barkhausen discontinuities are directly related.

Another interesting regularity appears in run nos. 8–13 and 41–45: Evidently in these cases the onset of Barkhausen signals has the character of a second *threshold of persistent hysteresis,* i.e., a region in which subsequent field cycles do *not* eliminate the Barkhausen jumps. Measurements show that the initial Barkhausen jumps on run nos. 8–13 and 41–45 do not occur at reproducible field points, but the graphical summary given on Fig. 4 indicates a well-defined clustering around a threshold value of $H_{\rm ext} \simeq 158$ mOe, or roughly $H_{\rm int} \sim 200$–$800\ \mu$Oe. The practical significance of this second threshold is that it sets a definite upper limit on the "interval of reversibility" that can be cleared of Barkhausen discontinuities in a few field sweeps. In this sense it provides a microscopic explanation for Rayleigh's H_U in Eq. (1.2).

Run nos. 8–15, 39, and 41–45 in Fig. 3 show another pattern of regularity: Whenever the second threshold is crossed on an ascending field sweep, Barkhausen jumps appear on the descending field sweep. Furthermore, the value of the field difference between the position of the maximum, or last, Barkhausen jump encountered on the ascending cycle and the position of the first Barkhausen jump encountered on the descending cycle is equal in magnitude to the second threshold field. Just as before, the pattern of the individual Barkhausen jumps is not reproducible. In fact, the actual field values of the gaps between the ascending and descending Barkhausen events may vary considerably. However, as shown in Fig. 4, the widths of these gaps are sharply defined, and, within our present experimental capability, indistinguishable from the magnitude of the second-threshold field.

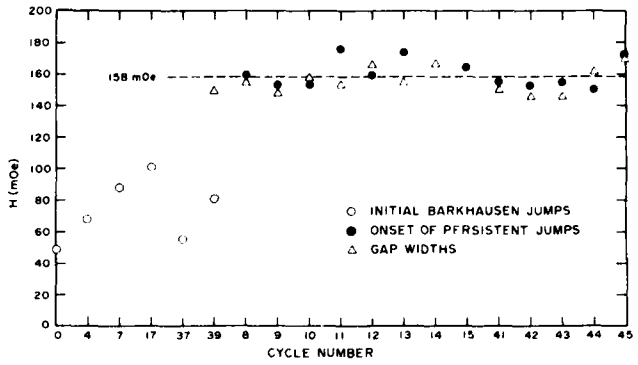

FIG. 4. Regularities of Barkhausen jumps. The open circles show the fields for which the first Barkhausen jump occurred on each ascending field of a cycle. The gap widths represent the field differences between the last Barkhausen jump for an ascending field and the first jump along the descending field of the same cycle.

The statistics are too sparse to draw any definite conclusions about a possible equipartition of Barkhausen jumps on the ascending and descending branches for field sweeps exceeding the second threshold. Nevertheless, detailed plots of the corresponding magnetization changes for repeated cycles exhibit a definite evolution from virgin to asymptotic hysteresis. For instance, between run no. 10 and run no. 13 the net change in the magnetization of the pill decreased by at least a factor of 17: In other words, run no. 10 corresponds to an open or incomplete loop on the I-H plane, whereas by the time run no. 13 was reached the loop had closed to within the gradiometer resolution.

The power-supply limitations discussed in Sec. II B prevented us from extending the range of field sweeps in a continuous manner beyond the maximum value of 367 mOe reached in run no. 10. Thus, as indicated in Fig. 3, we turned a vice into a virtue by employing auxiliary supplies to establish successive base fields at 250 and 500 mOe: In this fashion we reproduced Rayleigh's original scheme of stepwise field increases (cf. Sec. I B 4 and Ref. 6). The resulting experimental evidence is clear: In the entire low-field regime spanned by Fig. 3, that is, for fields in the range $10^{-6} \lesssim H_{\rm ext} \lesssim 1$ Oe, or equivalently, $10^{-8} \lesssim H_{\rm int} \lesssim 10^{-2}$ Oe, the precise value of the initial magnetization of the sample is irrelevant. Since, in any case, there are inherent limitations in the degree of demagnetization, as shown in Eq. (2.1), this is a useful result. However, the essential consequences lie deeper: *the fact that the entire pattern of first and second Barkhausen thresholds*—together with their associated memory effects—*can be exhibited in three different field regimes in run nos. 1–13, 14–17, and 36–45, each beginning with a different base field, shows that there are definite topographic regularities on the extended energy surfaces that describe the hysteresis.* This point is discussed in further detail in Sec. IV.

C. Energy losses in incipient hysteresis

The energy changes associated with magnetizing processes are usually represented as path-dependent vector

line integrals in the I-H plane,[3]

$$\mathcal{E} = V \int \vec{H}_{ext} \cdot d\vec{I} \ . \tag{3.4}$$

If the magnetization increments are split into reversible and irreversible components, then the energy also can be written in the form

$$\mathcal{E} = \mathcal{E}_{rev} + \mathcal{E}_{irr} \ , \tag{3.5a}$$

where the reversible component for a transition from an initial state (i) to a final state (f) is

$$\mathcal{E}_{rev} = V \int_i^f \vec{H}_{int} \cdot d\vec{I}_{rev} + \tfrac{1}{2} VN(|I_{rev}|_f^2 - |I_{rev}|_i^2) \ . \tag{3.5b}$$

As usual, V is the volume of the sample and N is the demagnetizing factor.

The energy dissipation is given by a discrete sum over Barkhausen jumps,

$$\mathcal{E}_{irr} = \sum_{j=1}^{n} |\Delta \vec{m}_j| \ |\vec{H}_{ext}(j)| \ . \tag{3.5c}$$

The transition from Eq. (3.4) to Eqs. (3.5b) and (3.5c) and its connection with Warburg's principle[33] for nonequilibrium processes is discussed in the Appendix.

In this subsection we present detailed results for the variation of $\mathcal{E}_{irr}$ based on the Barkhausen measurements displayed in Fig. 3. For each jump we measured the magnitude of the change in magnetic moment, $|\Delta \vec{m}_j|$, and the corresponding value of the field, $|\vec{H}_{ext}(j)|$, where the jump occurred. In order to focus on a specific example, the raw data for the ascending field sweep in run no. 10 are given in Table II. It should be cautioned that since $|\Delta \vec{m}_j|$ represents a change in the *bulk* magnetic moment of the sample, the actual energy dissipated at the domain level is different;[30] the precise correspondence would have to be established by calorimetric methods.

Since the number of Barkhausen jumps is an increasing function of the field, it is convenient to plot $\mathcal{E}_{irr}$ as a function of n, or, equivalently, $H_{ext}(n)$. A few trial graphs confirmed that the particular value of the base field was irrelevant. In fact, the essential trends in the data emerged most clearly when the threshold of Barkhausen emission in any given run was chosen as the origin for that particular run. For this purpose it is convenient to rewrite Eq. (3.5c) in the form

$$\mathcal{E}_{irr}(n) = \tilde{f}(n)[H_{ext}(n) - H_{ext}(1)] \ , \quad n > 1 \tag{3.6a}$$

where $H_{ext}(1)$ is the field where the initial Barkhausen jump occurs, and the auxiliary function $\tilde{f}(n)$ is given by

$$\tilde{f}(n) = [H_{ext}(n) - H_{ext}(1)]^{-1} \sum_{j=2}^{n} |\Delta \vec{m}_j| \ |\vec{H}_{ext}(j)| \ . \tag{3.6b}$$

When the data points are replotted according to Eqs. (3.6), one finds that $\mathcal{E}_{irr}(n)$ is a linear function of $H_{ext}(n)$ for all ascending field sweeps. This regularity suggests that one should normalize the slopes so that the energy variations due to the different base fields become less conspicuous. An obvious choice is the following:

$$\mathcal{E}_{irr}^{norm}(n) = f(n)[H_{ext}(n) - H_{ext}(1)] \ , \quad n > 1 \tag{3.7a}$$

where

$$\mathcal{E}_{irr}^{norm}(n) \equiv \mathcal{E}_{irr}(n)/H_{ext}(1) \ \text{ and } \ f(n) \equiv \tilde{f}(n)/H_{ext}(1) \ . \tag{3.7b}$$

In other words, the *normalized cumulative energy dissipation* $\mathcal{E}_{irr}^{norm}$ for any given run is simply the usual energy dissipation divided by the magnitude of the field where the first Barkhausen jump occurred on that particular run.

Figure 5 shows a compilation of plots of $\mathcal{E}_{irr}^{norm}(n)$ versus $H_{ext}(n) - H_{ext}(1)$ for ten distinct ascending hysteresis cycles. It is evident that in the range $0 \le H_{ext}(n) - H_{ext}(1) \le 210$ mOe, all of the data indicate that $f(n)$ is a *constant* with a value of about 6.6×10^{-6} erg/Oe^2. This "universal" linear behavior is a consequence of two further empirical regularities: (i) All of the Barkhausen jumps on Fig. 3 have roughly the same order of magnitude, and (ii) the spacing between the jumps does not vary erratically. The auxiliary function $f(n)$ can then be computed explicitly.

We first note that the sum in Eq. (3.6b) can be simplified because

$$|\Delta \vec{m}_j| \approx [\Delta m]_{av} \sim 1.13 \times 10^{-7} \text{ emu} \ , \tag{3.8a}$$

where the average change in magnetic moment was computed from data for all runs. Furthermore,

$$|\vec{H}_{ext}(j)| \cong H_{ext}(1) + (j-1)[\Delta H]_{av} \ , \quad [\Delta H]_{av} \sim 23 \text{ mOe} \tag{3.8b}$$

where the average field interval between jumps, $[\Delta H]_{av}$, also was obtained using all available data. It then is simple to show that

TABLE II. Cumulative energy losses in incipient hysteresis. Data for run no. 10 on Fig. 3.

	Barkhausen jump number (j)							
	1	2	3	4	5	6	7	8
$\lvert\Delta \vec{m}_j\rvert$ (10^{-7} emu)	1.00	1.15	1.23	1.15	1.15	1.00	1.12	1.00
$\lvert\vec{H}_{ext}(j)\rvert$ (mOe)	154	174	195	227	246	274	295	345
$H_{ext}(j) - H_{ext}(1)$	0	20	41	73	92	120	141	191
$\mathcal{E}_{irr}^{norm}(n)$	1[a]	2.29	3.85	5.55	7.39	9.17	11.3	13.6

[a]Equation (3.6b) is undefined for $n = 1$; however, the normalized energy dissipation for the initial jump can be obtained directly from Eq. (3.5c).

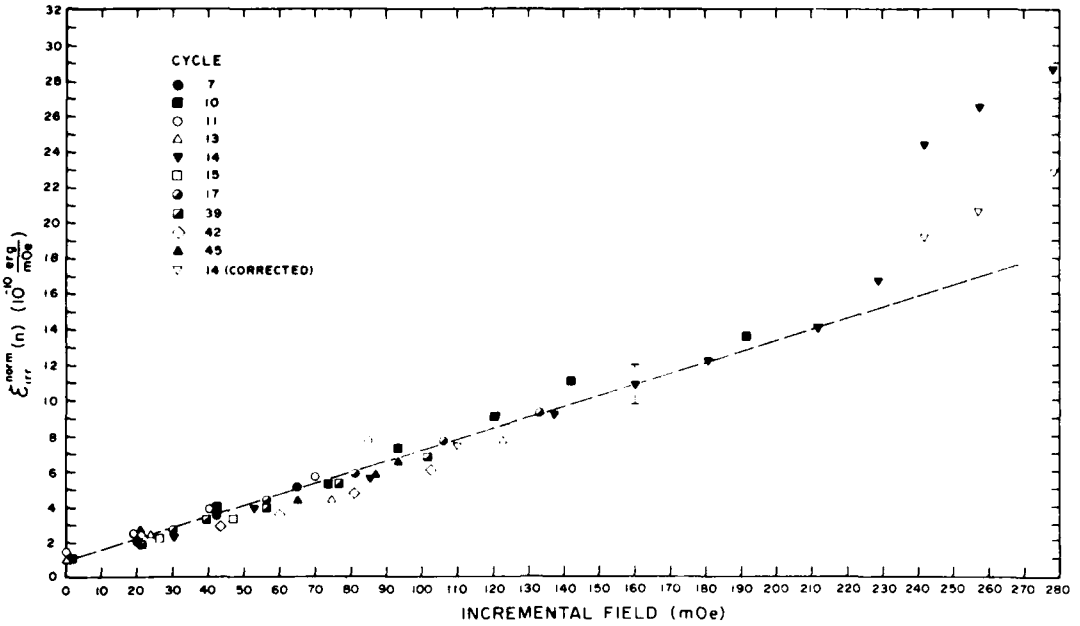

FIG. 5. Variation of hysteresis energy with magnetic field. The normalized energy dissipation defined in Eq. (3.7b) is plotted along the ordinate. For each cycle the incremental field is measured from the initial Barkhausen jump. The experimental accuracy is indicated by the error bar for the 160-mOe point. At 242 mOe there was a burst of noise that may have obscured a Barkhausen jump; the "corrected" points were obtained by combining all other data for cycle no. 14 with Eq. (3.9).

$$f(n)=\frac{[\Delta m]_{\rm av}}{[\Delta H]_{\rm av}}\left[\left[1-\frac{[\Delta H]_{\rm av}}{H_{\rm ext}(1)}\right]\frac{n}{n-1}+\frac{n[\Delta H]_{\rm av}}{2H_{\rm ext}(1)}\frac{n+1}{n-1}\right]. \tag{3.9}$$

The fact that $f(n)$ is scaled by the ratio of the averages $[\Delta m]_{\rm av}/[\Delta H]_{\rm av}$ is dimensionally obvious. However, the terms in the large square brackets are more interesting: In particular, it is finally clear that the basic reason for the linear behavior in Fig. 5 is that *the threshold for Barkhausen jumps is much greater than the interval between jumps.* Specifically, for all the runs above the second threshold we have the upper bound $[\Delta H]_{\rm av}/H_{\rm ext}(1)\sim 0.14$. It is then easy to check that for moderate values of n the expression in large square brackets in Eq. (3.9) is nearly constant, i.e., $f(n)\sim 6.7\times 10^{-6}$ erg/Oe^2; this agrees with the average slope found in Fig. 5.

The second term in large square brackets in Eq. (3.9) indicates that for field excursions where $n[\Delta H]_{\rm av}$ becomes comparable to $2H_{\rm ext}(1)$, the linear variation of $\mathscr{E}_{\rm irr}(n)$ with $H_{\rm ext}(n)$ will fail. This is indeed the case for run no. 14 where $n=14$, $n[\Delta H]_{\rm av}=278$ mOe, and $2H_{ext}(1)=508$ mOe. For extremely high field sweeps where $n[\Delta H]_{\rm av}\gg 2H_{\rm ext}(1)$—in other words, for field excursions far above the Barkhausen threshold—the cumulative energy dissipation in Eq. (3.7a) becomes a *quadratic* function of the field. It is plausible that this may be the underlying reason for the quadratic component of the Jordan-Gans law, Eq. (1.11).

Finally, it can be shown that the cumulative energy dissipation for the descending field sweeps in Fig. 3 is given by an analogous expression:

$$\mathscr{E}_{\rm irr}^{\rm norm}(n)=g(n)\,|\,H_{\rm ext}(n)-H_{\rm ext}^{-}(1)\,|\ , \tag{3.10a}$$

where

$$g(n)=\frac{[\Delta m]_{\rm av}}{[\Delta H]_{\rm av}}\left[\left[1+\frac{[\Delta H]_{\rm av}}{H_{\rm ext}^{-}(1)}\right]\frac{n}{n-1}-\frac{n\,[\Delta H]_{\rm av}}{2H_{\rm ext}^{-}(1)}\frac{n+1}{n-1}\right]. \tag{3.10b}$$

In this case the index "1" refers to the first Barkhausen jump encountered as the field is decreased; the corresponding field value is $H_{\rm ext}^{-}(1)$. This simple change in convention has an important physical consequence: For the descending field sweeps one *always* ends with the condition $n[\Delta H]_{\rm av}\approx H_{\rm ext}^{-}(1)$, and therefore Eqs. (3.10) will always have significant nonlinear components.

D. Hysteresis in an iron whisker

The onset of hysteresis in weak magnetic fields was also observed in the iron whisker sample described in Sec. II C. For these experiments the 1.72-cm axis of the whisker was oriented coaxially with the SQUID gradiometer coils and the sample placed in contact with the Dewar bottom. In order to minimize Barkhausen emission and internal fields in the whisker, the transverse magnetization shown in Fig. 1 was used for most measurements. According to Eq. (2.4) the internal field is then approximately given by

$$H_{\rm int}\simeq 4\pi H_{\rm ext}/\mu N_{\perp}\sim H_{\rm ext}/10^{3}\ , \tag{3.11}$$

where the permeability of the whisker is $\mu\sim 2000$ and the transverse demagnetizing factor is $N_{\perp}\sim 2\pi$. The Braunbeck coil system and operational amplifiers described in

Sec. II B provided controlled field sweeps in the interval $10^{-6} \lesssim H_{ext} \lesssim 0.3$ Oe. Fixed base fields of 0.3 and 0.6 Oe were used to extend the upper limits to 0.9 Oe. The evolution of the whisker hysteresis was followed in 96 magnetization cycles roughly paralleling the sequence shown in Fig. 3.

In the lowest field range, 1 μOe $\lesssim H_{ext} \lesssim$ 20 mOe, the magnetization of the whisker was linear and reversible. This behavior is consistent with the results obtained for the pill sample in Sec. III A.

For field excursions up to 200 mOe the magnetization remained linear within $\pm 2\%$ but showed a hysteresis. The corresponding triangular magnetization pattern is sketched in Fig. 8(c). The hysteresis had a memory dependence analogous to the magnetic Kaiser effect described in Sec. III B 3. This behavior is illustrated with several examples in Table III. For instance, the top row of the table summarizes the measurements for run $m=1$. This was the *first* time, after a whisker demagnetization, that the field was increased from 0 to 31.5 mOe. As indicated by the slope in column 4, the associated gradiometer flux increased by $(387 \pm 2.5)\Phi_0$, where $\Phi_0 = 2.07 \times 10^{-7}$ G cm^2 is the flux quantum. When the field was reduced to zero, the gradiometer flux decreased by $(374 \pm 2.5)\Phi_0$, leaving a net flux change of $(13 \pm 5)\Phi_0$. The second ($m=2$) row of the table indicates that the next field cycle terminated at a somewhat lower peak value, 0→27.3 mOe→0, and this time the hysteresis was essentially quenched. A similar pattern appeared in all further field cycles. Invariably there was a net flux change on the mth cycle if $H_{ext}(m)$ exceeded the field maxima attained on *all* previous cycles. The entries for $m=38$ and 51 in Table III indicate that this memory effect persisted during at least 13 intermediate-field excursions. On the other hand, if the peak field decreased, that is, if $H_{ext}(m) > H_{ext}(m+1)$, then the net flux change on the $(m+1)$st cycle was very small or vanished altogether. This quenching is illustrated by the entries for $m=2$, 17, 39, 52, 69, and 80 in Table III.

The Kaiser-like behavior of the hysteresis and memory effects continued with regularity up to the highest field levels that could be reached by combining the 367-mOe sweep field with a 600-mOe base field. In addition, above 200 mOe, field cycles with hysteresis showed a nonlinearity of the magnetization on the initial up sweeps [cf. Eq. (1.9) and footnote c of Table III]. Sporadic Barkhausen jumps of the order of $(10-50)\Phi_0$ occurred above 500 mOe. In all cases, two or three repeat cycles at lower field levels tended to restore linear and reversible behavior in the magnetization.

The crucial point of the low-field whisker hysteresis is that it represents *irreversible behavior without any observable Barkhausen discontinuities.* Estimates similar to those given in Sec. III B 1 show that the largest Barkhausen signals that could have escaped detection by the SQUID gradiometer–strip-chart recording system would be flux jumps of about $0.5\Phi_0$, corresponding to magnetic moment changes of 10^{-7} emu in the whisker. This implies, for example, that if the whisker hysteresis on the lowest-field run ($m=1$ on Table III) were entirely due to unobserved Barkhausen jumps, then there must have been at least six of these discontinuities. Similar estimates can be derived from the data for other field cycles.

If these "invisible" Barkhausen jumps really existed, and it were possible to eliminate them by successive field sweeps following the pattern of Fig. 3, then the Kaiser-like behavior of the whisker and pill hysteresis could be traced to a common origin. The differences between the "Up" and "Down" slopes of the magnetization in Columns 4 and 5 of Table III would then also have to be ascribed to the cumulative effects of these invisible jumps, cf. Sec. I B 3. Although the possibility of such an ultrami-

TABLE III. Magnetic hysteresis in an iron whisker.

Run no. (m)	Maximum field [$H_{ext}(m)$] (mOe)	Net flux change (in units of Φ_0)	Up slope[a] (Φ_0/mOe)	Down slope[b] (Φ_0/mOe)
1	31.5	13±5	12.3	11.9
2	27.3	0±5	11.2	11.2
15	127.5	0±5	11.9	11.7
16	214.2	115±5	12.8[c]	12.2
17	198.5	18±5	12.3	12.2
38	288	146±9	11.8[c]	11.4
39	235	0±9	11.7	11.8
51	318	129±5	11.8[c]	11.5
52	317	44±5	12.0	11.4
68[d]	383[e]	84±2	4.3[c]	3.1
69	371[e]	2.7±2	3.3	3.2
79	657[f]	106±2	4.8[c]	3.2
80	645[f]	4.4±2	3.2	3.1

[a](Gradiometer flux)/(external field), increasing H_{ext}.

[b]As above, decreasing H_{ext}.

[c]Average slope; the susceptibility is not constant.

[d]For all $m > 64$, the whisker end was moved 1.2 cm below the Dewar; this diminished the flux at the gradiometer by a factor of 2.5.

[e]For $68 \leq m \leq 78$ the base field was 300 mOe.

[f]For $79 \leq m \leq 87$ the base field was 600 mOe.

croscopic regime of Barkhausen noise has been mentioned in the literature,[11,14] extensive studies of magnetic domains in iron whiskers point in the opposite direction: Bitter patterns of carefully grown pure whiskers with few defects show large domains with well-defined wall deformations.[34,35] Recent SQUID measurements of Barkhausen signals from iron whiskers also show only isolated large jumps ($\gtrsim 10^4\Phi_0$) in fields above 0.1 Oe.[28] Similar results have been obtained with the whisker used in the present experiments when the external field was oriented *parallel* to the 1.72-cm axis.

A new interpretation of the origin of the whisker hysteresis is given in the next section.

IV. HYSTERESIS THEORY

The magnetic hysteresis and memory effects displayed by the iron pill and whisker samples are consequences of a general phenomenology of hysteresis.[36] This theory also accounts for the changes in energy dissipation that occur during the transition from virgin to asymptotic hysteresis. Since the first systematic investigations by Ewing in the 1880's it has been known that the effects of hysteresis can be simulated by irreversible transitions among sets of metastable states in magnetic dipole systems (Ewing arrays[37,38]). This classical picture has been refined by quantum mechanics and modern theories of domain formation, but transitions between metastable states are still at the core of all current theories of hysteresis.[14] In this section we give a brief review of the standard model of magnetic hysteresis[15,39] and discuss the generalizations that are associated with the memory and energy dissipation effects.

A. Standard model

It is usually assumed that the states of a magnetic material can be characterized by a free-energy sum

$$V(q_j)=\sum_i V_i(q_j) \tag{4.1}$$

which includes contributions from structural features such as (i) the crystalline energy, (ii) the anisotropy energy, (iii) strain energy, (iv) exchange energy, (v) magnetostatic energy, and (vi) domain-wall energy.[3] The configuration coordinates q_j denote wall displacements, pinning sites, spin aggregates, and other variables that specify the states of the system. The domain configurations can then, in principle, be obtained from the variational problem

$$\delta V=0 \text{ , or } \frac{\partial V}{\partial q_j}=0 , \tag{4.2a}$$

with the local stability constraint that the Hessian matrix

$$\mathcal{H}(q)=\frac{\partial^2 V}{\partial q_j\,\partial q_k} \tag{4.2b}$$

is positive definite.

If an external magnetic field is applied, the domain configurations may change. The response of the system is usually treated by perturbation methods. It is assumed that after the field is switched on, the total energy is given by

$$V_T(H,q_j)=-HI_s\sum_k v_k\cos\phi_k+V(q_j) , \tag{4.3}$$

where $V(q_j)$ is the material energy from Eq. (4.1), and the magnetic interactions are summed over all the domain volumes v_k. As usual I_s denotes the saturation magnetization, and ϕ_k is the angle between the field and the magnetization of the kth domain. The changes in the domain structure can then be obtained from the equilibrium condition

$$\delta V_T(H,q_j)=\delta V(q_j)-HI_s\sum_k \delta(v_k\cos\phi_k)=0 , \tag{4.4}$$

in analogy with Eq. (4.2a).

The simplest illustration of these external-field effects is provided by the shift of a single 180° domain wall. Suppose this wall is parallel to the y-z plane and separates two domains in the shape of square prisms with a common cross-sectional area L^2. If the wall moves through a distance δx, the variation of the magnetic energy is $2HI_sL^2\cos\phi\,\delta x$. In this special case, Eq. (4.4) reduces to

$$H=(2I_sL^2\cos\phi)^{-1}\frac{dV}{dx} , \tag{4.5}$$

which, in principle, furnishes an explicit relation between the field strength and the wall displacements.

Useful qualitative results can be obtained even if the detailed variation of $V(x)$ is unspecified. Figure 6(a) shows how Barkhausen jumps and hysteresis effects appear in cases where dV/dx is not monotonic. To be specific, suppose that the wall is initially at point a. As indicated on the figure, this is an equilibrium position with $H=dV/dx=0$. For systems with one degree of freedom the Hessian stability criterion [Eq. (4.2b)] reduces to

$$\frac{d^2V_T}{dx^2}=\frac{d^2V}{dx^2}>0 , \tag{4.6}$$

and, therefore, a also marks a position of stable equilibrium. If the field is switched on and allowed to vary in the range $0=H(a)\le H<H(b)$, the wall will shift to new equilibrium positions determined by Eq. (4.5). According to Eq. (4.6), all of the displacements in the interval $0=x(a)\le x<x(b)$ are stable and reversible. Clearly, this simple model reflects the reversible magnetization observed in the pill and whisker samples at the lowest field levels, particularly on run nos. 1–3 in Fig. 3.

The field $H(b)$ is an upper bound for this region of reversibility. Figure 6(a) shows that all wall positions in the interval $x(b)\le x\le x(d)$ are unstable, and therefore as soon as the field reaches $H(b)$ the system will jump to another point of stable equilibrium. This discontinuous transition is indicated on the figure by the dashed line extending from b to c. Physically, this jump corresponds to the first Barkhausen signal observed on run no. 4 in Fig. 3. If the field is decreased again, the wall will shift through the stable region $x(c)\to x(d)$, and finally jump from d to e. The inset on the right-hand side of Fig. 6(a) shows how repeated field variations can build up a complicated hysteresis network of smooth and discontinuous domain transformations.

This hysteresis model has been extended in two directions:

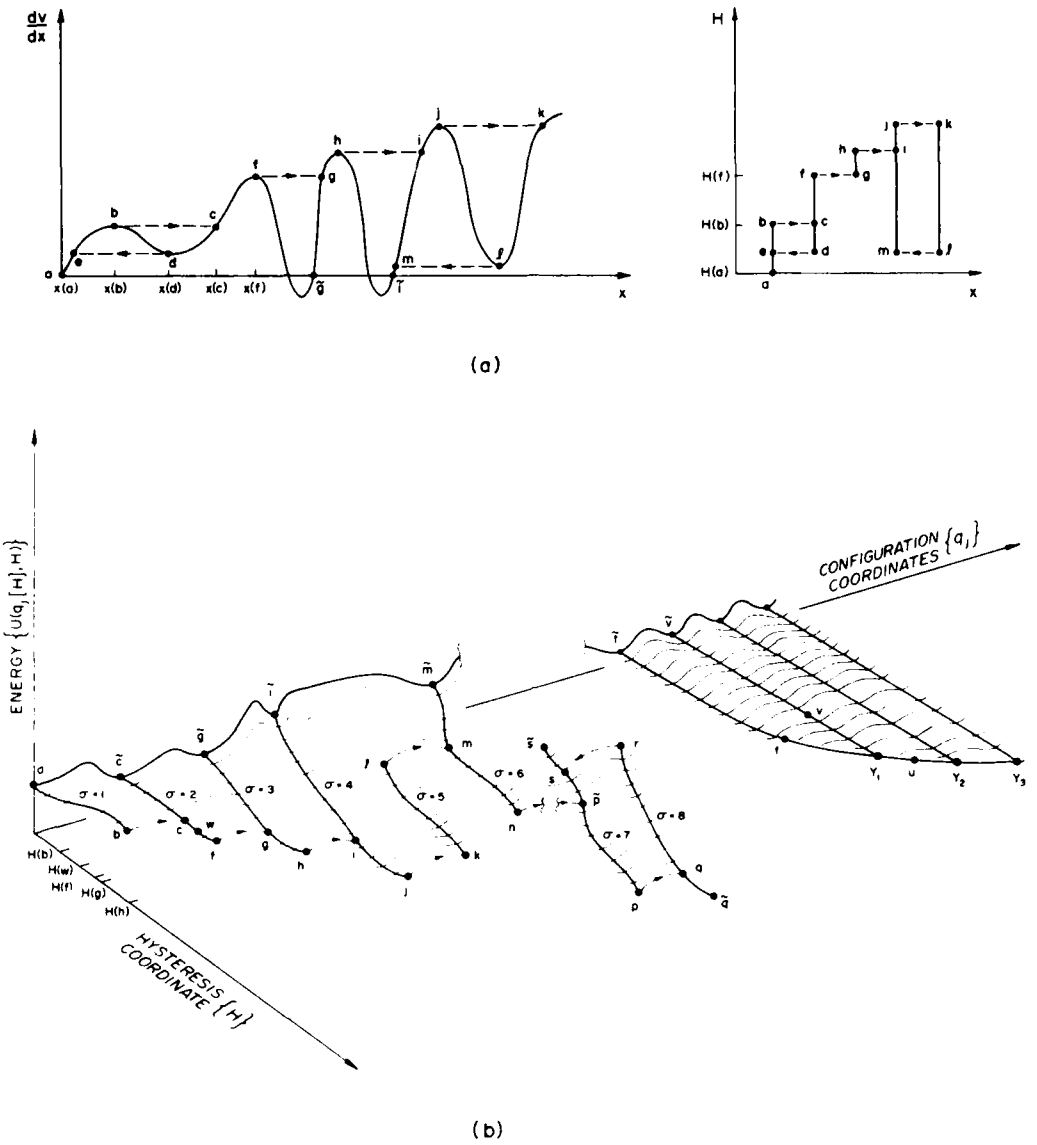

FIG. 6. (a) Standard model of hysteresis. The extremals of the dV/dx curve are points of instability where jumps occur [Eqs. (4.5) and (4.6)]. The corresponding hysteresis network is shown on the right. (b) Hysteresis energy manifold. The stability valleys indicate regions of reversible behavior. The exothermic jumps are denoted by dashed lines. The Y points are bifurcations of stability valleys. The Kaiser effect is a consequence of the distribution of instability points in the H-q_j (hyper)plane.

(1) The domain dynamics implicit in Eqs. (4.4) and (4.5) have been checked by many experiments with simple systems.[40] For example, in selected monocrystals, estimates of the free energy derived from band-structure calculations can be correlated with the observed wall dynamics.[3,11] However, this contact with solid-state physics is far removed from the practical problems of hysteresis in bulk ferromagnets.

Neel was among the first to suggest that statistical methods might bridge this gap.[15]

(2) The basic idea is to replace a complicated Hamiltonian by a random Hamiltonian. This approximation is useful in many other situations, e.g., structural mechanics and nuclear physics,[41] even though its justification is still unclear and no error bounds are available. Neel introduced this stochastic element in the hysteresis model by assuming that *the free energy* in Eq. (4.1) *is a random variable*. In practical terms this means that for every wall position x the corresponding value of dV/dx is to be understood as a *probability density* with a Gaussian distribution. In addition, the random variables associated with x and $x + nl$, $n = 1,2,\ldots$, are all assumed to be independent. (For technical reasons it is necessary to discretize the wall displacements.) The essential consequence is that Eq. (4.5) now becomes a relation between an experimentally determined field H and the ensemble average $\langle dV/dx \rangle$. The corresponding total free energy, $V_f(H,x)$ in Eq. (4.3), is equivalent to an ensemble of potential wells characterized by a mean depth or "activation field" H_a. For fields that are weak in the sense that $H \ll H_a$, the

Gaussian ensemble averages can be approximated by simple polynomials. Equation (4.5) can then be inverted and combined with Eq. (4.3) to give a relation between the average magnetic moment and the field, i.e.,

$$\langle \mu \rangle \sim I_s L^2 \langle x \rangle \propto H + H^2 + \cdots . \tag{4.7}$$

This expansion is equivalent to Eq. (1.9) and is the principal result of the statistical hysteresis theory.[3,11,15]

B. General hysteresis

The systematic extinction of Barkhausen jumps (or magnetic Kaiser effect) and the regular hysteresis patterns shown in Figs. 3 and 4 imply that the magnetic free energy of the polycrystalline iron sample used in our experiments is *not* a random variable. A similar conclusion follows from the Barkhausen memory effects observed in gadolinium.[32] A comparison of Figs. 3 and 6(a) shows that the structure of the dV/dx curve is almost completely determined by the regularities of the Barkhausen jumps and the constraints of Rolle's theorem. For instance, the disappearance of the jumps on run nos. 4–8 and 37–41 is reflected in the sequence of increasing maxima f, h, and j. The return sweeps to zero field are represented by the points $\tilde{g}$ and $\tilde{i}$. Run nos. 8 and 9 correspond to the hysteresis cycle $j \to k \to l \to m$, etc. However, this procedure has its practical limits. If all 134 Barkhausen jumps in Fig. 3 were mapped onto the dV/dx curve in Fig. 6(a), the resulting tangle of lines would obscure all traces of the underlying hysteresis patterns.

This information is presented in a clearer format in Fig. 6(b). By introducing the magnetic field as an extra dimension, the criss cross of Barkhausen jumps is avoided and the evolution of the hysteresis is laid out in the form of a space-time diagram. The total energy $U(q[H],H)$ also differs from the perturbed energy $V_I(H,q)$ of the standard model. We recall that a basic assumption of the perturbation treatment is that the free energy of the material determines the locally stable domain configurations, and that the only effect of a varying external field is to induce transitions among this set of *predetermined* states. However, this approximation can fail even in simple classical systems. Detailed studies of Ewing arrays show that external fields, lattice distortions, etc. can create entirely *new* domain structures and most of the hysteresis is due to transitions among these nonperturbative states.[38]

These complications are taken into account in the general hysteresis theory by replacing Eqs. (4.1)–(4.4) with the variational condition

$$\frac{\partial U(q_j[H],H)}{\partial q_j} = 0 , \tag{4.8}$$

where U is the total energy of the system in the presence of the external field, and the configuration coordinates may have an explicit field dependence. Since multiple solutions will always occur in hysteresis systems, it is convenient to label the extremals of Eq. (4.8) with a separate index σ, i.e.,

$$q_j^\sigma = q_j^\sigma(H), \quad \sigma = 1,2,\ldots . \tag{4.9}$$

The subset of locally stable states can then be identified with the help of the Hessian. As before, in Eq. (4.2b), this means that the matrix

$$\mathcal{H}(H,\sigma) = \frac{\partial^2 U}{\partial q_j^\sigma \partial q_k^\sigma} \tag{4.10}$$

is positive definite. Barkhausen jumps and quasireversible transitions (see below) occur whenever this Hessian becomes singular, i.e.,

$$\det | \mathcal{H}(H,\sigma) | = 0 . \tag{4.11}$$

If H is varied, the system will move along the stable σ extremals and change states at the nodes determined by Eq. (4.11). The resulting hysteresis networks are usually quite complex because the determinant is practically always a complicated function of the field H. The general hysteresis theory is discussed in detail in Refs. 36 and 38.

C. Memory effects and hysteresis cycles

The magnetic Kaiser effect can now be given a simple graphical interpretation with the help of Fig. 6(b). Suppose we begin with the pill sample after a demagnetization: In Fig. 3 this state is represented by the initial point on cycle no. 1; in Fig. 6(b) it corresponds to the local minimum at a. If the field is now cycled between $0 \le H < 68.9$ mOe, the reversible magnetization on run nos. 1–4 is represented in Fig. 6(b) by reversible motion in the *local stability trough* between a and b. The Barkhausen jump at 68.9 mOe on run no. 4 terminates this interval of reversibility. In Fig. 6(b) this transition corresponds to the end of the $\sigma = 1$ stability trough at b—a singularity of the Hessian. At this point the system "rolls" down the energy surface (corresponding to an exothermic domain transformation) and reequilibrates at c in a new stability trough. The remaining field increase from 68.9 to 74.7 mOe on cycle no. 4, then prods the system from c to w in the $\sigma = 2$ track.

It is apparent from Fig. 3 that no Barkhausen jumps occur during the field decrease (74.7→0 mOe) on run no. 4. This implies that on the *next* field increase on run no. 5 the system *must* retrace its path in the $\sigma = 2$ trough. Escape from a stability valley is only possible at a singularity of the Hessian. The absence of jumps means that Eq. (4.11) does not have this kind of instability between $\tilde{c}$ and w. Magnetization measurements also exclude quasireversible forks (cf. Sec. IV D). The essential conclusion is that *the first Barkhausen jump on track $\sigma = 2$ must occur at a higher field value than $H(w)$, or $H(b)$, on track $\sigma = 1$—this monotonic progression of singularities is the essence of the Kaiser effect.* The succeeding field cycles confirm this picture in detail. For instance, on run no. 5 the peak field was 70.9 mOe, i.e., less than $H(w)$, and on run no. 6 the peak field was adjusted to reproduce $H(w)$—no Barkhausen jumps occurred on either cycle. However, on the next cycle (no. 7) the field was raised to higher levels, and jumps appeared at 88, 108, 130, and 153 mOe. Since no jumps were observed during the field decrease, this monotonic progression should continue. Indeed, on run no. 8 the first Barkhausen jump on the ascending cycle occurred at 158 mOe. A similar progression is exhibited by cycle nos. 36–39.

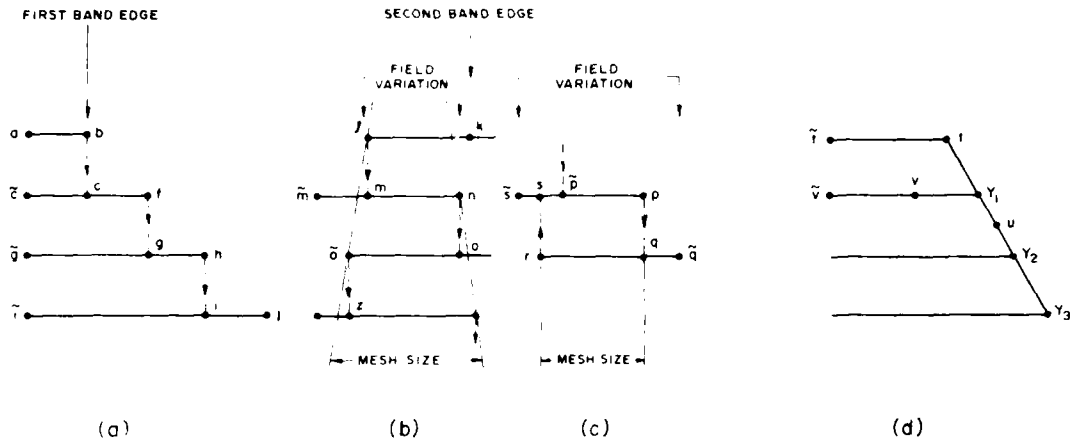

FIG. 7. (a) Kaiser effect in Barkhausen jumps. The hysteresis network is a projection of the $a-\tilde{l}$ stability valleys of Fig. 6(b) on the H-q plane. The first band edge is the onset of irreversibility (Ref. 36). (b) Fading or drifting hysteresis. The diverging dotted-dashed lines indicate an increase of the average interval between instabilities. In this case the Barkhausen jumps and energy dissipation gradually diminish as the number of cycles increases. The second band edge marks the beginning of persistent hysteresis. (c) Steady or asymptotic hysteresis. If the field variations match the mesh size, the system will be trapped in the loop. The associated energy dissipation will remain constant from cycle to cycle. (d) Kaiser effect in bifurcations. Hysteresis without Barkhausen jumps.

The memory dependence of Barkhausen jumps is displayed by the hysteresis network in Fig. 7(a). This diagram is a projection of the energy surface in Fig. 6(b) on the H-q_j plane. Although the precise location of the nodal points $a-j$ is determined by the characteristics of the pill sample, the overall pattern of these transitions has a general significance: The same type of memory effect appears in the hysteresis of dipole arrays,[36,38] the shakedown of frames in structural mechanics,[36,42] and of course in acoustic emission, i.e., the Kaiser effect.[25–27]

The first Barkhausen jump on a decreasing field sweep appears on cycle no. 8. According to Fig. 6(b), this corresponds to a transition such as l to m. Consequently, during the next field increase on cycle no. 9, the system traverses a new stability valley ($\sigma=6$). There are no *a priori* bounds on the location of the next singular point n, and therefore the corresponding field $H(n)$ does not have to exceed $H(k)$. In other words, *jumps on descending field sweeps signal the end of the Kaiser effect.* Pasztor and Schmidt found the same "failure" of the Kaiser effect in their acoustic emission studies (cf. cycle no. 7 on Fig. 7 of Ref. 27).

Figures 3 and 4 indicate that beyond the first "band edge" of the Kaiser effect new kinds of hysteresis patterns appear: (1) The threshold of Barkhausen emission tends to occur at the same field level from cycle to cycle, and (2) for any given cycle the difference in field between the *last* Barkhausen jump seen during the field increase and the *first* Barkhausen jump on the field decrease also tends to be constant. In fact, it is numerically equal to the threshold value found in (1). Figures 6(b) and 7(c) show that this characteristic field, which happens to be approximately 158 mOe for the pill sample, can be interpreted as the average *mesh* size of the hysteresis network on the energy surface. The difference in the pattern of Barkhausen jumps on the ascending and descending field cycles on Fig. 3 is a consequence of this mesh structure. Quantitatively, this means that there are regularities in the field differences, e.g.,

$$H(j)-H(l)\approx H(n)-H(l)\approx H(p)-H(r)\approx 158\ \text{mOe}\ . \tag{4.12}$$

The basic significance of the mesh size is displayed in Figs. 7(b) and (c); these also represent projections of the energy surface of Fig. 6(b) on the H-q_j plane. *A necessary condition for persistent hysteresis is that the variation of the applied field exceeds the mesh size.* The simplest illustration is provided by the isolated hysteresis loop $p\rightarrow q\rightarrow r\rightarrow s$ on Figs. 6(b) and 7(c). This loop is entered via a Barkhausen jump at $\tilde{p}$. If the subsequent field variation is smaller than the mesh size, the system will respond reversibly. Run no. 40 in Fig. 3 is an experimental example. For field variations comparable to the mesh size but bounded by $H(\tilde{s})$ and $H(\tilde{q})$, the system is trapped in this loop and will exhibit an invariant (that is, asymptotic) hysteresis. Still larger field variations may decant the system into other stability troughs, and the hysteresis will drift.

Figure 7(b) shows the simplest idealization of drifting hysteresis. In this case the number of Barkhausen jumps will slowly *decrease* as the field is cycled between fixed limits. Eventually the system will migrate to a region of the energy surface where the mesh size is larger than the field variation, and complete reversibility is restored. Point z marks such a cycle in Fig. 7(b). Experimentally, this dramatic extension of reversibility is exhibited by run nos. 60, 65, and 66 in Fig. 3. Additional examples of drifting hysteresis are discussed in Refs. 36, 38, and 42.

D. Hysteresis without Barkhausen jumps

In n-dimensional spaces the instability criterion [Eq. (4.11)] can lead to many different types of singularities or "catastrophes." Discontinuous transitions such as Barkhausen jumps or acoustic emission pulses are the easiest to detect experimentally and therefore have received the most attention. However, the network sketched in Fig. 7(d) shows that instability and irreversibility can

also arise from simple bifurcations. Studies of magnetic dipole systems (or Ewing arrays) confirm that hysteresis can result from the bifurcation of stability valleys on the energy surface.[36,38] This situation is illustrated on the right-hand side of Fig. 6(b): Suppose that the system is initially in a state represented by point $\tilde{t}$. Then, for all field cycles between $0 \leq H \leq H(t)$, the system will respond reversibly by moving in the stability trough between $\tilde{t}$ and t. If the field is increased further—so that the system reaches u—and then is decreased again, the one-to-one correspondence between fields and states is broken, because, at the bifurcation point Y_1, the system can continue either on the old $t-\tilde{t}$ track, or on the new $v-\tilde{v}$ track.

It is plausible that the iron whisker hysteresis described in Sec. III D is due to domain bifurcation. This phenomenon would provide a mechanism for irreversible magnetization without Barkhausen jumps. In particular, the reversibility that is observed at low fields and the Kaiser-like behavior of the hysteresis at higher fields can be accounted for by supposing that the whisker hysteresis occurs in a network resembling that of the pill sample. In both cases the instabilities are ranged in an increasing field sequence, i.e., $H(b)<H(f)$, etc. and $H(Y_1)<H(Y_2)$, etc. The essential difference is that in the whisker case the jumps are replaced by bifurcation [cf. Figs. 6(b) and 7(d)].

At the domain level, bifurcations and Barkhausen jumps both involve the coherent transition of at least 10^{10} electrons. In this sense each instability point on Fig. 6(b) actually represents an ensemble of transformations of the underlying density matrices. This implies, in particular, that if the bifurcation Y_1 is crossed in a *decreasing* field cycle, the choice between the $t-\tilde{t}$ track and the $v-\tilde{v}$ track is governed by a probability distribution. The changes in the whisker magnetization shown on Table III reflect, in part, the evolution of this probability distribution.

E. Energy dissipation

Stochastic elements also appear in energy dissipation. In the standard model they enter via Eq. (4.7), and, as shown in Ref. 15, lead to Rayleigh's cubic law of hysteresis losses [Eq. (1.10)]. However, the results of Jordan,[16] Gans,[17], Ellwood,[9] Baldwin,[18] and the measurements reported in Sec. III C all indicate that the energy losses in low-field hysteresis are proportional to the first and second powers of the field. Baldwin[19] has shown that these power laws are incompatible with Eq. (4.7).

The variation in these power laws can be derived from the general hysteresis theory. According to Eq. (3.5c), the energy dissipation is given by a discrete sum over Barkhausen jumps. If we rewrite this equation in the form

$$\mathcal{E}_{\rm irr}=\sum_{j=1}^{n} e_j \ , \tag{4.13}$$

where e_j is the energy dissipated at the jth jump, it becomes clear that the basic problem is to find a connection between the total number of jumps n and the field variation $H(t)$. Figure 6(b) suggests a geometrical version of this problem. Suppose that at time t_0 the system is at some initial point $H(t_0)$, $q_j(H(t_0))$ on the energy surface. Subsequent variations of H will then induce a wandering of the system through the hysteresis network. If $\mathscr{P}(H(t_0), H(t))$ denotes the path traversed during the interval $t-t_0$, the energy losses can be determined by summing Eq. (4.13) over all the jumps encountered along $\mathscr{P}$. Since $\mathscr{P}$ is generally a functional of the *entire field history* between t_0 and t, the explicit computation of $\mathcal{E}_{\rm irr}$ is difficult.

The experimental power laws for the energy dissipation can now be obtained with the simplifying assumption that the hysteresis networks are sufficiently large so that the path "length" $l(\mathscr{P})$ can be estimated by statistical methods. Basically, this means replacing Eq. (4.13) by the average energy dissipation

$$\langle \mathcal{E}_{\rm irr} \rangle = \langle \rho l(\mathscr{P}) \rangle \ , \tag{4.14}$$

where ρ is the number of jumps per unit path length.[36,38] In order to evaluate Eq. (4.14), it is necessary to assign a metric to the energy surface so that distances and lengths can be computed. Furthermore, the ensemble of paths between fixed end points must be endowed with a probability measure so that average path lengths can be determined. These technical problems can be resolved with the help of the theory of probabilistic metric spaces.[43] The end result is that the average energy loss is given by

$$\langle \mathcal{E}_{\rm irr} \rangle = c_1(H-H_b)+c_2(H-H_b)^2+c_3(H-H_b)^3 \ , \tag{4.15}$$

where H_b is the field at the band edge, cf. Figs. 7(a) and (b); and the ratios of the coefficients c_i are scaled by the distance between the initial and final points on the energy surface.[44] It can be shown under quite general conditions that in virgin hysteresis the linear and quadratic terms dominate; in these cases, $H_b \to H_t$, the field marking the threshold of irreversible behavior. Similarly, it can be shown that in asymptotic hysteresis [Fig. 7(c)] the cubic term dominates.[36] Needless to say, Eq. (4.15) provides a general setting for the energy-loss results previously given in Eqs. (3.7a)–(3.10b).

V. SUMMARY AND CONCLUSIONS

The questions raised in Sec. I C can now be answered as follows:

(a) For very slow field sweeps ($\sim 1\ \mu$Oe/sec) in the range $1-187\ \mu$Oe, the magnetization in polycrystalline samples of pure iron, at room temperature, is reversible and without any discernible Barkhausen emission above a noise level of about 3×10^{-8} emu. (*Note added*: Similar behavior is observed in nickel.)

(b) In polycrystalline samples of iron there is a sharp demarcation between reversible and irreversible magnetization: This transition coincides with the appearance of Barkhausen jumps. The onset of magnetic hysteresis also coincides with the threshold of Barkhausen emission. Within the experimental errors, the total changes in magnetization can be accounted for by superposing the Barkhausen jumps and the reversible components of magnetization.

(c) Repeated field cycles in the threshold region of

Barkhausen emission remove the jumps and extend the range of reversible magnetization: This quenching phenomenon is equivalent to a magnetic Kaiser effect.

(d) The energy losses in incipient or drifting hysteresis are proportional to $(H-H_t)+(H-H_t)^2$, where H_t is the field at which the first Barkhausen jump occurs.

(e) In the field range 20–500 mOe, iron whiskers exhibit magnetic hysteresis without any detectable Barkhausen signals.

ACKNOWLEDGMENTS

We would like to thank Dr. M. Rubinstein [Naval Research Laboratory (NRL)], Dr. P. Lubitz (NRL), and Professor R. V. Coleman (University of Virginia) for supplying the samples and helpful advice. We also thank Dr. J. H. Claassen (NRL) for the loan of some electronic equipment. We are grateful to Messrs. C. Harris and R. Bender (NASA Goddard Space Flight Center) for assistance with the measurements. Professor J. S. Kouvel (University of Illinois, Chicago) kindly provided access to a vibrating-sample magnetometer for auxiliary measurements. We thank as well Dr. M. Camras, P. Everett, and Professor S. J. Putterman for informative conversations. This work was supported in part by the U. S. Office of Naval Research, the Naval Research Laboratory, (Washington D. C.) and the Research Corporation. The majority of the work of H.W. was performed at the Naval Research Laboratory under Contract No. N00014-82-K-2042.

APPENDIX: EXTENSIONS OF WARBURG'S PRINCIPLE

If the magnetization energy [Eq. (3.4)] is evaluated for a hysteresis cycle, the formal result is the loop integral

$$\delta_W = V\oint \vec{H}_{\rm ext}\cdot d\vec{I}\ . \tag{A1}$$

It was first suggested by Warburg[33] that under steady-state conditions, δ_W represents the irreversible energy losses per cycle. This equivalence between the areas of hysteresis loops and energy dissipation is exploited in many practical applications, but its limits of validity are unclear. For instance, in low-field hysteresis, Ellwood's measurements showed that the areas of hysteresis loops and the energy dissipation were different.[9] Similarly, in high fields, the experiments of Tebble *et al.*[22,23] and of Koller *et al.*[24] demonstrated that there were large discrepancies between the areas of hysteresis loops and cumulative Barkhausen energy losses (Sec. I B 3). The pattern of Barkhausen jumps observed in the present experiments also poses a problem: It is difficult to see how a *linear* law of energy dissipation such as Eq. (3.7a) can be associated with the area of a loop in the I-H plane.

Barkhausen jumps are tacitly included in the magnetization energy by interpreting (A1) as a Stieltjes integral. This point is illustrated by the inset labeled "Stieltjes" in Fig. 8(a). This represents an enlargement of the hysteresis loop $\tilde{V}-V$ in the vicinity of one of the vertices. As usual, the transition from the lower to the upper branch of the magnetization curve is presumed to occur via Barkhausen jumps—these are indicated on the figure by the vertical lines. For practical calculations it is convenient to consider the simplest case: a hysteresis loop in the form of a parallelogram bounded by two jumps. Experimentally, this situation corresponds to run nos. 8, 9, and 41 in Fig. 3; on Fig. 6(b) it is represented by the loop $s\to p\to q\to r$. If for the moment we ignore the angular dependence implicit in (A1), the magnetization energy for the cycle shown on Fig. 8(b) is

$$\oint \vec{H}\cdot d\vec{I} \to \int_s^p H\,dI + \int_q^r H\,dI \quad \text{(reversible contribution)} \tag{A2a}$$

$$+\Delta\delta(p\to q)-\Delta\delta(r\to s) \quad \text{(Stieltjes contribution)}\ , \tag{A2b}$$

where

$$\Delta\delta(p\to q)=H(p)\,|\,I(q)-I(p)\,|\ ,\quad \Delta\delta(r\to s)=H(s)\,|\,I(s)-I(r)\,|\ . \tag{A2c}$$

Geometrically, it is obvious that Eqs. (A2) yield the area of the parallelogram. However, this result is only obtained if the two Stieltjes contributions partially cancel. In other words, irrespective of the sign conventions for exothermic and endothermic processes, one jump must represent an energy gain and the other an energy loss. This concept clashes with the standard model of Barkhausen jumps presented in Sec. IV. Below the magnetic domain level there are microscopic degrees of freedom associated with the damping of wall movements, thermal fluctuations, zero-point fluctuations, etc. The irreversibility of Barkhausen transitions is a consequence of the fact that the jumps always transfer energy into these microscopic degrees of freedom. The inadequacy of the Stieltjes picture also follows from the occurrence of "negative" Barkhausen jumps: In these cases a field increase causes a jump with decreasing magnetization and *vice versa*.[12] Several jumps of this type were observed during the course of the present experiments.

The exothermic picture of Barkhausen jumps is indicated in the upper inset on Fig. 8(a). The macroscopic hysteresis loop $\tilde{V}-V$ is now represented by an aggregate of disjoint curve fragments, each fragment corresponding to an interval of reversible magnetization. The Barkhausen jumps link these fragments, but the result is not a closed curve on the I-H plane. In this picture the energy flow consists of reversible and irreversible components as in Eq. (3.5a). Specifically,

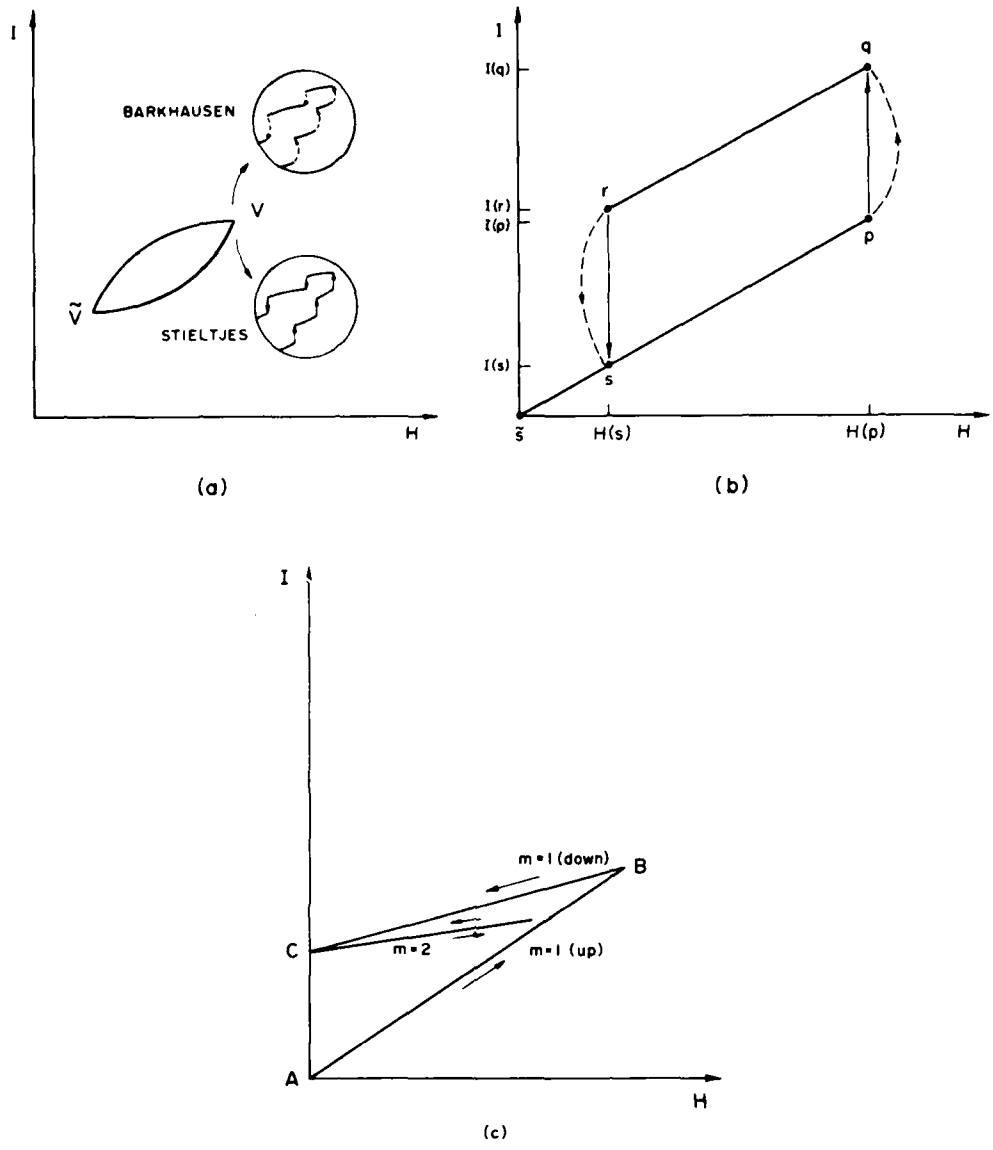

FIG. 8. (a) Macroscopic and microscopic hysteresis. The insets show two idealizations of irreversible domain transformations. The differences are explained in the Appendix. (b) Hysteresis cycle bounded by two Barkhausen jumps. The two vertical lines $r \rightarrow s$, and $p \rightarrow q$ represent jumps in the Stieltjes picture, Eqs. (A2). In the Barkhausen picture the energy transfer during a jump does not correspond to a locus on the I-H plane. (c) Hysteresis of an iron whisker. The diagram shows the magnetization for runs $m = 1$ and 2 in Table III. Cycle no. 1 had a net magnetization change proportional to $\sim 13\Phi_0$; this is represented by the interval $A-C$. The hysteresis disappeared on subsequent cycles ($m \geq 2$) to lower peak fields.

$$\delta = V \sum_{\substack{\text{curve} \\ \text{fragments}}} \int \vec{H} \cdot d\vec{I} \quad \text{(reversible contribution)} \tag{A3a}$$

$$+ \sum_j e_j \quad [\text{irreversible (Barkhausen) contribution}] , \tag{A3b}$$

where Eq. (A3b) coincides with Eqs. (3.5c) and (4.13). If these expressions are evaluated for the hysteresis cycle in Fig. 8(b), the reversible components in Eqs. (A2a) and (A3a) are equal, but the irreversible parts of Eqs. (A2b) and (A3b) differ by a minus sign, i.e.,

$$\sum_j e_j = V[\Delta\delta(p \rightarrow q) + \Delta\delta(r \rightarrow s)] . \tag{A4}$$

Evidently, the total energy budget of Eqs. (A3) is not related to the area of a loop.

Warburg inferred the connection between energy dissipation and the loop integral in Eq. (A1) by applying the first law to a cyclic magnetization process. If we drop the cyclic assumption, we are left with the weaker constraint

$$\delta_i(\text{total energy input}) \geq \delta_{\text{irr}}(\text{Barkhausen losses}) . \tag{A5}$$

In the particular case of the parallelogram cycle in Fig. 8(b), the reversible energy input—Eqs. (A2a) or (A3a)—vanishes, and Eq. (A5) reduces to a tautology. However, the experimental picture is different. For example, on run no. 8 in Fig. 3, the Barkhausen energy losses were 3×10^{-7} erg/cm^3, and the slopes of the increasing and de-

creasing field cycles were both measured to be $0.29 = I/H_{ext} \simeq N_t^{-1}\ [1-(N_t\chi)^{-1}]$ (Sec. III B 1). It is easy to check that a susceptibility difference of $\delta\chi/\chi^2 \sim 3\times 10^{-4}$ would be sufficient to account for the Barkhausen losses. The precision of the slope measurements would require improvement by 4 *orders of magnitude* to detect this difference. At higher field levels, Barkhausen emission increases, and it is easier to distinguish reversible and irreversible energy dissipation (cf. Sec. 9.7.5 of Ref. 3).

Since hysteresis in bulk ferromagnets involves transitions among many metastable states, it is difficult to check when cyclic or steady-state conditions, i.e., asymptotic hysteresis, have been reached. This evolution of hysteresis can also be modeled by Ewing arrays. One then can see in detail that it is easy to counterfeit the closure of a hysteresis loop. The external field and the magnetization are cycled, but the system does *not* have to return to its initial state because there may be many metastable states that have the same magnetization.[36] In these non-equilibrium situations the energy and magnetization are highly degenerate functions of the configuration coordinates [cf. Eq. (4.8) and (4.9)] and therefore cannot satisfy any relation of the type $\mathscr{E} = \mathscr{E}(I)$, etc.[45] Warburg's principle is valid only when the system returns to its initial microstate. Under these circumstances the first law [Eq. (A5)] reduces to an equality and it becomes feasible to relate the reversible and irreversible energy losses in hysteresis. It is plausible that engineering estimates of energy dissipation—say, for transformers—can be related to the areas of hysteresis loops, because in asymptotic hysteresis [Fig. 7(c)] the systems approximately retrace the same set of microstates during each cycle.

Finally, in Fig. 8(c) we show the hysteresis pattern for the iron whisker corresponding to runs $m = 1$ and 2 in Table III. By virtue of the Kaiser effect there is a net energy transfer to the whisker during run no. 1; this is represented by the area of the triangle *ABC*. As indicated in Sec. III D, this is an example of hysteresis without loops or any discernible Barkhausen emission.

---

*Present address: Air Force Office of Scientific Research/ Electronics and Materials Science Department, Bolling Air Force Base, Washington, D.C. 20332.

†Present address: Department of Physics, University of California at Los Angeles, Los Angeles CA 90024.

[1]R. Becker, Z. Phys. **62**, 253 (1930).
[2]F. Bloch, Z. Phys. **74**, 295 (1932).
[3]E. Kneller, *Ferromagnetismus* (Springer, Berlin, 1962).
[4]J. J. Brophy, in *Fluctuation Phenomena in Solids*, edited by R. E. Burgess (Academic, New York, 1965), pp. 1–35.
[5]G. Ferrari, J. L. Porteseil, and R. Vergne, IEEE Trans. Magn. **MAG-14**, 764 (1978).
[6]J. W. Strutt (Baron Rayleigh), Philos. Mag. **23**, 225 (1887).
[7]A. Koller, Z. Angew. Phys. **23**, 161 (1967).
[8]A. Koller, E. Pfrenger, and K. Stierstadt, J. Appl. Phys. **39**, 869 (1968).
[9]W. B. Ellwood, Physics (J. Appl. Phys.) **6**, 215 (1935).
[10]H. D. Bush, Nature (London) **166**, 401 (1950).
[11]R. Vergne, J. C. Cotillard, and J. L. Porteseil, Rev. Phys. Appl. **16**, 449 (1981).
[12]K. Stierstadt, *Der Magnetische Barkhausen Effekt*, Vol. 40 of *Springer Tracts in Modern Physics*, edited by G. Höhler (Springer, Berlin, 1966), pp. 2–106.
[13]M. Lambeck, *Barkhausen Effekt* (de Gruyter, Berlin, 1971).
[14]M. Kléman, J. Phys. (Paris) **42**, 1263 (1981).
[15]L. Néel, Cahiers Phys. **12**, 1 (1942).
[16]H. Jordan, Elek. Nachr. Tech. **1**, 7 (1924).
[17]R. Gans, Ann. Phys. (Leipzig) **20**, 701 (1933).
[18]J. A. Baldwin, Jr., J. Revol, and F. Milstein, Phys. Rev. B **15**, 426 (1977).
[19]J. A. Baldwin, Jr., IEEE Trans. Magn. **MAG-14**, 81 (1978).
[20]J. A. Baldwin, Jr. and F. Milstein, J. Appl. Phys. **44**, 4739 (1973).
[21]G. Montalenti, Nuovo Cimento **5**, 154 (1948).
[22]H. D. Bush and R. S. Tebble, Proc. Phys. Soc. London **60**, 370 (1948).
[23]R. S. Tebble, I. C. Skidmore, and W. D. Corner, Proc. Phys. Soc. London **63**, 739 (1950).
[24]A. Koller, Z. Angew. Phys. **24**, 164 (1968).
[25]J. Kaiser, Arch. Eisenhüttenwesen **24**, 43 (1953).
[26]C. Schmidt and G. Pasztor, IEEE Trans. Magn. **MAG-13**, 116 (1977).
[27]G. Pasztor and C. Schmidt, J. Appl. Phys. **49**, 886 (1978).
[28]C. Heiden and H. Rogalla, J. Magn. Magn. Mater. **19**, 240 (1980).
[29]K. Warmuth, Arch. Elektrotechnik **33**, 747 (1939).
[30]C. Heiden and L. Storm, Z. Angew. Phys. **21**, 349 (1966).
[31]R. M. Bozorth and J. F. Dillinger, Phys. Rev. **41**, 345 (1932).
[32]T. Erber, J. L. Porteseil, and P. Molho, Memory Dependence of Barkhausen Emission (Grenoble, 1982) (unpublished).
[33]E. Warburg, Ann. Phys. (Leipzig) **13**, 141 (1881).
[34]G. Lidgard and W. D. Corner, IEEE Trans. Magn. **MAG-2**, 499 (1966).
[35]P. W. Shumate, R. V. Coleman, and R. C. Fivaz, Phys. Rev. B **1**, 394 (1970).
[36]T. Erber, S. A. Guralnick, and H. G. Latal, Ann. Phys. (N.Y.) **69**, 161 (1972).
[37]J. A. Ewing, *Magnetic Induction in Iron and Other Metals* (Electrician Printing and Publishing Co., London, 1894).
[38]T. Erber, B. N. Harmon, and H. G. Latal, Adv. Chem. Phys. **20**, 71 (1971).
[39]M. Kersten, *Grundlagen einer Theorie der ferromagnetischen Hysterese und der Koerzitivkraft* (Hirzel, Leipzig, 1943).
[40]H. J. Williams and W. Shockley, Phys. Rev. **75**, 178 (1949).
[41]C. E. Porter, *Statistical Theories of Spectra: Fluctuations* (Academic, New York, 1965).
[42]S. A. Guralnick, S. Singh, and T. Erber, Jr., Struct. Eng. **110**, 2103 (1984).
[43]B. Schweizer and A. Sklar, *Probabilistic Metric Spaces* (North-Holland, New York, 1983).
[44]T. Erber, B. Schweizer, and A. Sklar, Commun. Math. Phys. **20**, 205 (1971).
[45]F. Pokropp, *Aggregation von Produktionsfunktionen* (Springer, Berlin, 1972).

END

FILMED

2-86

DTIC